AGING IMMUNE SYSTEM

B cells drive CD4 T cell immunosenescence and age-associated health decline

Saad Khan[1,2,3]†, Mainak Chakraborty[2,3]†, Fei Wu[4], Nan Chen[2,3,5], Tao Wang[6,7,8], Yi Tao Chan[1,2,3], Azin Sayad[9], Max Kotlyar[10], Faisal J. Alibhai[7], Minna Woo[1,2,3,11], Ren-Ke Li[7,12], Mansoor Husain[5,6,7,8], Igor Jurisica[10,13,14], Adam J. Gehring[1,15], Pamela S. Ohashi[1,9], David Furman[4], Sue Tsai[16], Shawn Winer[5,17]‡, Daniel A. Winer[1,2,3,4,5]*‡

Dysregulation of the adaptive immune system is a key feature of aging and is associated with age-related chronic diseases and mortality. Here, we find that T cell aging, especially in the CD4 subset, is controlled by B cells. B cells contributed to the age-related reduction of naive CD4 T cells, their differentiation toward immunosenescent T cell subsets, and age-associated T cell receptor clonal restriction. Concurrently, mice lacking B cells displayed improvements in health span and life span. We uncovered a role for B cell–intrinsic insulin receptor signaling in influencing age-related B cell phenotypes that in turn induces CD4 T cell dysfunction, a process that is in part driven by major histocompatibility complex class II. These results identify B cells as critical mediators driving age-associated adaptive immune dysfunction and health-span outcomes and suggest previously unrecognized modalities to manage aging and related health decline.

INTRODUCTION

Aging is associated with a gradual decline in tissue and organ function, often resulting in chronic complications and diminished survivability (*1*, *2*). The unprecedented growth of the global aged population (>65 years) is of great concern, given that the elderly display the highest death rate linked with major noncommunicable diseases, such as cardiovascular disease, type 2 diabetes, and Alzheimer's disease (*3*). One important contributor to the aging process is the development of chronic low-grade inflammation, termed "inflammaging," that progressively increases and is linked to the onset of age-related complications and decreased survival of the elderly (*4*, *5*). Immune cells are central to inflammaging, and age-related changes in the immune system are collectively termed "immunosenescence" (*6*). Immunosenescence is directly responsible for age-related increases in basal levels of inflammation, decreased vaccine efficacy, and increased susceptibility to pathogens (*6*, *7*).

The adaptive immune system shows key features of immunosenescence. T cells display a loss in their naive pool and an expansion of memory subsets, which is concurrent with a loss in overall T cell receptor (TCR) diversity (*8*, *9*). Mechanisms, including thymic involution, hematopoietic stem cell insufficiency, altered homeostatic proliferation, and intrinsic T cell defects, are believed to limit naive and quiescent-like T cell states (*8*, *10*–*14*). Concurrently, there is an increase in differentiated effectors, such as effector memory–like (T_{EM}), exhausted, T follicular helper (T_{FH}), and senescent-like T cell subsets, which cumulatively contribute to inflammaging, senescence, and tissue deterioration during aging (*14*). These mechanisms are further complicated by apparent heterogeneity in CD4 and CD8 T cell aging because of variations in naive cell peripheral homeostasis, TCR signaling, cellular metabolism, and epigenetic modifications (*15*–*17*).

Concurrently, aging is associated with a decline in early B cell progenitors and a shift away from a naive dominant B cell compartment toward one that displays greater features associated with activation, including increased production of proinflammatory cytokines, memory-associated phenotypes, terminal differentiation toward antibody secreting cells, and the development of a hypermetabolic age-associated B cell (ABC) subset that expresses increased inflammatory and antigen presentation machinery (*18*–*22*). In health and disease settings, B cells are modulators of T cell function, via antigen presentation, activation, polarization, and generation of memory responses (*23*, *24*). CD4 T cell activation and memory response induction often occur through interaction with B cells, whereas CD8 T cell memory responses often occur independently of B cells (*25*–*27*). Whether B cells in aged organisms contribute to CD4 and CD8 T cell immunosenescence remains to be determined.

Here, we demonstrate that the presence of B cells across the mouse life span influences the composition of the T cell compartment, their activation state, and inflammatory potential, as well as their overall TCR repertoire, findings which are linked with parameters of longevity and health span. We uncover a role for the insulin receptor (InsR) in mediating its proaging effects on mice by acting on B cells

[1]Department of Immunology, University of Toronto, Toronto, ON M5S 1A8, Canada. [2]Division of Cellular and Molecular Biology, Diabetes Research Group, Toronto General Hospital Research Institute (TGHRI), University Health Network, Toronto, ON M5G 1L7, Canada. [3]Banting and Best Diabetes Centre, University of Toronto, Toronto, ON M5G 2C4, Canada. [4]Buck Institute for Research on Aging, 8001 Redwood Boulevard, Novato, CA 94945, USA. [5]Department of Laboratory Medicine and Pathobiology, University of Toronto, ON M5S 1A8, Canada. [6]Department of Physiology, University of Toronto, ON M5S 1A8, Canada. [7]Toronto General Hospital Research Institute (TGHRI), University Health Network, Toronto, ON M5G 1L7, Canada. [8]Ted Rogers Centre for Heart Research, Toronto, ON M5G 1X8, Canada. [9]Princess Margaret Cancer Centre, University Health Network, ON M5G 2C1, Canada. [10]Osteoarthritis Research Program, Division of Orthopedic Surgery, Schroeder Arthritis Institute, University Health Network, and Data Science Discovery Centre for Chronic Diseases, Krembil Research Institute, Toronto, ON M5T 0S8, Canada. [11]Division of Endocrinology and Metabolism, Department of Medicine, University Health Network, University of Toronto, ON M5G 1L7, Canada. [12]Division of Cardiac Surgery, University Health Network, University of Toronto, ON M5G IL7, Canada. [13]Departments of Medical Biophysics and Computer Science and Faculty of Dentistry, University of Toronto, ON M5S 2E4, Canada. [14]Institute of Neuroimmunology, Slovak Academy of Sciences, Bratislava, Slovakia. [15]Toronto Center for Liver Disease and Schwartz Reisman Liver Research Centre, Toronto General Hospital Research Institute (TGHRI), University Health Network, Toronto, ON M5G 1L7, Canada. [16]Department of Medical Microbiology and Immunology, University of Alberta, Edmonton, AB T6G 2RS, Canada. [17]Department of Pathology and Laboratory Medicine, Mount Sinai Hospital, Toronto, ON M5G 1X5, Canada.
†These authors contributed equally to this work.
‡These authors contributed equally to this work.
*Corresponding author. Email: dan.winer@uhn.ca

to promote ABC phenotypes and drive T cell immunosenescence and reduced health span. We show that B cells particularly influence CD4 T cell dysfunction, which proceeds in a major histocompatibility complex class II (MHCII)–dependent manner. Overall, these findings link an endocrine signaling axis with dysfunctional adaptive immunity and declining health parameters with age.

RESULTS

B cell deficiency prevents age-related alterations to splenic T cells

We first documented baseline levels of age-related changes in B and T cell populations by flow cytometry (fig. S1, A and B) in spleens of aged (range: 22 to 30 months) C57BL6/J female wild-type (WT) mice in our facility. $CD19^+$ $B220^{hi}$ (B2) cells are the majority B cell fraction essential for humoral immunity, T cell activation, and immunological memory (*28*–*30*). Among total B cells, $B220^{lo/-}$ and $B220^{hi}$ subsets remained unchanged, whereas in the B2 fraction, we observed an age-associated decline in the frequency of follicular B cells (FOBs) and a concurrent expansion of a $CD21^-$ $CD23^-$ fraction, previously described as ABCs (*21*), as well as $CD11c^+$ T-bet^+ B2 cells (fig. S2, A to D). Concurrent assessment of the aged T cell compartment confirmed a strong decrease in the frequency of naive T cells and an expansion of T_{EM} cells and exhausted $PD1^+$ T cells (fig. S2, E and F), which were independent of alterations to the frequency or cellularity of total splenic T cells or the proportion of total CD4 and CD8 T cells (fig. S2, G and H). Cumulatively, these results are in line with previous observations regarding the aged adaptive immune compartment.

Given the functional relevance of B cells in influencing T cell phenotypes across a variety of health and age-related disease states (*23*, *24*, *31*), we hypothesized that aged mice lacking B cells would display alterations in the composition of their splenic T cell compartment. Thus, we aged B cell–deficient (μMT) mice to ~24 months (fig. S2I) (*32*). As a result of B cell deficiency, the relative abundance of splenic T cells increased in μMT mice, despite an overall decrease in cellularity, compared with WT controls (fig. S2J). In addition, in the T cell compartment, there was an increase in the relative abundance of CD8 T cells and a reduction in the relative abundance of CD4 T cells (fig. S2K).

To further probe the composition of the T cell compartment, we performed 5′ single-cell RNA sequencing along with VDJ TCR sequencing on sorted $CD3^+$ cells from the spleens of aged μMT and WT mice. Uniform Manifold Approximation and Projection (UMAP) reduction revealed 13 clusters found in both conditions, and on the basis of expression patterns of *Sell*, *Ccr7*, *Cd44*, *Pdcd1*, and *Tox*, we were able to annotate major cell clusters as naive T cells (clusters 0 and 3), exhausted and effector memory (Ex/Mem) T cells (clusters 1 and 6), and central memory T cells (T_{CM} cells) (clusters 2 and 7) (Fig. 1, A and B, and fig. S2L). The remaining clusters displayed several features that prevented them from being annotated as traditional naive T cells, Ex/Mem T cells, or T_{CM} cells. These included Foxp3-expressing regulatory T cells (T_{reg} cells) (cluster 4) and natural killer T cells (NKT cells) (clusters 5 and 11), as well as T cells that displayed distinct gene expression patterns including an interferon gene signature (*Isg15*, *Ifit1*, and *Ifit3*—cluster 8), myeloid-like features (*Apoe* and *C1qb*—cluster 9), proliferation markers (*mKi67* and *Top2a*—cluster 12), and mixed immune cell genes, which likely represent additional CD3-expressing populations (*H2-Aa* and *S100a9*—cluster 10) (Fig. 1, A and B, and fig. S2L).

Aged μMT mice had a splenic T cell compartment that appeared to resist aging-related changes. In the aged μMT T cell pool, we observed marked increases in the relative abundances of naive CD4 (cluster 3) and CD8 (cluster 0) T cells, as well as pronounced reductions in the relative abundances of Ex/Mem CD4 (cluster 1) and CD8 (cluster 6) T cells (Fig. 1C). Similar effects were observed after analysis by flow cytometry (Fig. 1D and fig. S2M). Concurrently, we also observed a decrease in the proportions of $PD1^+$ T cells (Fig. 1E and fig. S2N) and splenic T_{reg} cells in the μMT T cell pool (Fig. 1F), as well as in T_{FH} cells (Fig. 1G). Conversely, in young mice, we observed minor differences in the composition of the splenic T cell compartment between WT and μMT mice (fig. S3, A to F). Accordingly, we observed that fold changes over time in splenic naive and age-related T cell subsets still were much more pronounced in WT mice during the aging process compared with age-matched μMT mice (fig. S3, G to K).

Given these differences in the composition of the T cell compartment between aged WT and μMT mice, we hypothesized that B cells might also be responsible for the altered T cell clonality and the loss in TCR diversity with age, major hallmarks of T cell aging. Analysis of the VDJ TCR sequences unveiled that at baseline (clonality = 1), T cells from aged μMT mice displayed higher diversity and markedly reduced clonal expansion (clonality > 1) compared with WT T cells with age (Fig. 1H). When superimposed upon our UMAP, the increase in T cell clonal expansion with age in WT mice was distinctly linked largely with T_{CM}, Ex/Mem, and T_{reg} cell clones, confirming that differentiation of naive cells toward these fates is responsible for a shrinking TCR repertoire (Fig. 1H). In mice lacking B cells, very few T cell clones were able to expand with age, creating a diverse TCR repertoire. Together, these findings suggest that B cells facilitate T cell adoption of an immunosenescent fate and TCR restriction with age.

B cell deficiency limits T cell inflammatory function during aging

We next sought to better understand how B cells may be modulating the splenic T cell compartment with age. We first explored whether the large changes in relative abundances of naive and major differentiated Ex/Mem T cell subsets may be associated with any differences in thymic output. Unexpectedly, these changes occurred in the absence of any alterations to thymic involution, thymocyte number, or T cell development (Fig. 2, A and B), indicating that B cells might be responsible for regulating the T cell compartment in the periphery rather than altering thymic output or developmental pathways.

Subsequently, we assessed differentially expressed genes (DEGs) between splenic T cells from aged WT and μMT mice (Fig. 2C). WT T cells displayed up-regulated expression of various identified aging-related genes (*Izumo1r*, *Tigit*, *Lag3*, *Gzmk*, *S100a11*, *Itga4*, *Tox*, *Pdcd1*, and *Aw112010*), whereas μMT T cells up-regulated genes found commonly in young T cells (*Satb1*, *Lef1*, and *Ccr7*). Accordingly, WT T cells expressed higher levels of genes traditionally associated with inflammatory/memory T cells (*CD44*, *CD38*, *Nrp1*, *Ier3*, *Sostdc1*, *Ly6a*, *Il21*, *Tnf*, and *Ifng*), whereas μMT T cells up-regulated genes linked with naiveness and quiescence (*CD55*, *Sell*, and *Dapl1*). In addition, in WT T cells, we observed higher expression of genes linked with (i) TCR signaling and antigen-presenting cell–mediated activation (*Lck*, *Zap70*, *Icos*, *Cd82*, *Tnfrsf4*, *Ctla4*, *Cxcr5*, and *Nr4a1*), (ii) transcription factors involved in T cell differentiation (*Maf*, *Foxp3*, *Rora*, *Bcl6*, *Batf*, *Ikzf2*, *Hif1a*, and *Bhlhe40*), and (iii) T cell senescence (*Cdkn1a*, *Cdkn1b*, and *Cdkn2a*). At the

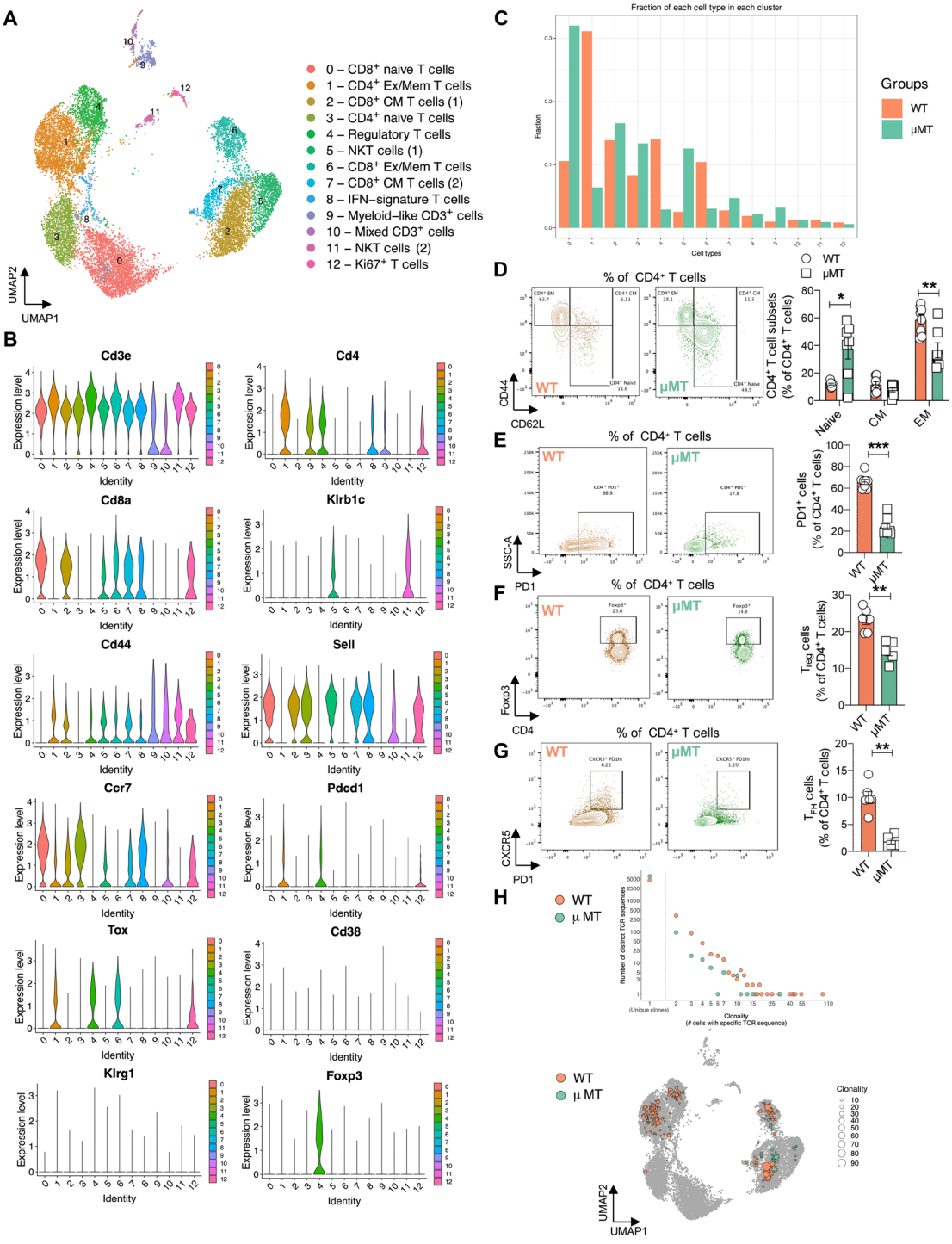

Fig. 1. Mice lacking B cells display reduced T cell immunosenescence. (**A** to **C**) 5′ Single-cell transcriptomics with VDJ TCR analyses on splenic CD3$^+$ cells from 24-month-old aged µMT and WT mice ($n = 2$ pooled cohoused mice per group). (A) UMAP and annotation of splenic CD3$^+$ clusters from aggregated aged µMT and WT mice. (B) Gene expression violin plots from aggregated aged µMT and WT mice. (C) Relative abundances of each cluster from µMT and WT mice. (**D** to **G**) Flow cytometric assessment of T cells from spleens of aged µMT and WT mice ($n = 5$ to 8 per group). (D) Representative plots (left) and relative abundances (right) of naive T cells, T_{EM} cells, and T_{CM} cells among CD4$^+$ T cells. (E) Representative plots (left) and relative abundances (right) of PD1$^+$ cells among CD4$^+$ T cells. (F) Representative plots (left) and relative abundances (right) of T_{reg} cells. (G) Representative plots (left) and relative abundances (right) of T_{FH} cells. (**H**) TCR diversity and clonality analysis of bulk (top) and TCR clonality overlaid on UMAP projection of CD3$^+$ clusters (bottom) from 5′ single-cell transcriptomics with VDJ TCR analyses on splenic CD3$^+$ cells from aged µMT and WT mice (two pooled cohoused mice per group). All experiments were repeated at least twice except for (A) to (C) and (H), which were obtained via a single experiment. Statistical difference between two means was determined via a Mann-Whitney test. Data are means ± SEM. *$P < 0.05$, **$P < 0.01$, and ***$P < 0.001$.

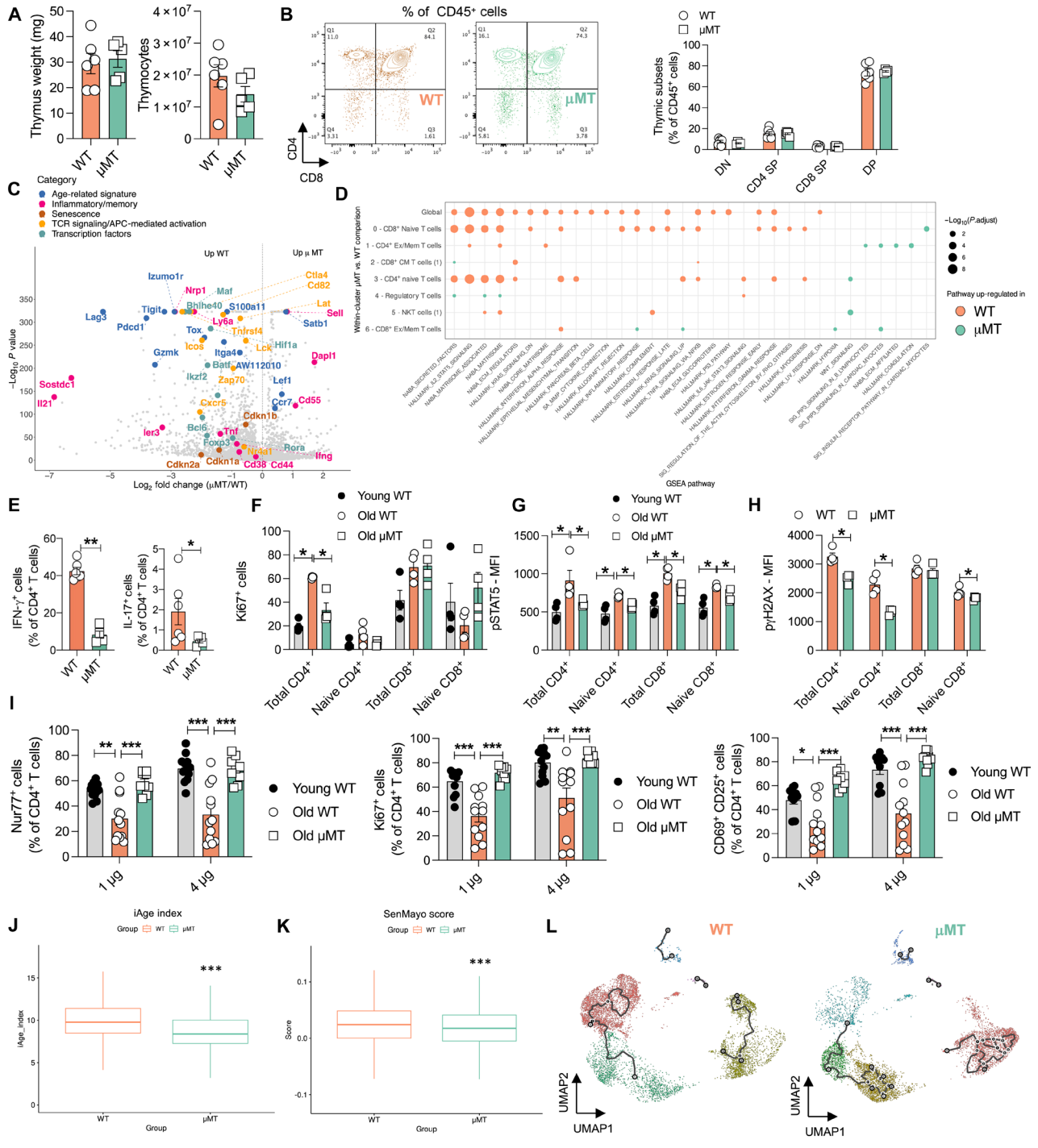

Fig. 2. B cell deficiency limits T cell inflammatory functional capacity. (**A**) Thymus weights (left) and thymocyte yields (right) and (**B**) representative plots (left) and relative abundances (right) of thymic T cell subsets from aged μMT and WT mice (n = 4 to 6 per group). (**C**) Volcano plot of genes globally up-regulated and (**D**) GSEA pathway analysis in CD3$^+$ cells from aged μMT and WT mice (n = 2 pooled cohoused mice per group). (**E** to **H**) Flow cytometric assessment of T cells from spleens of aged μMT and WT mice (n = 4 to 6 per group). (E) Relative abundances of IFN-γ$^+$ cells (left) and IL-17$^+$ cells (right) among CD4$^+$ T cells after 5-hour ex vivo stimulation. (F) Frequencies of proliferating Ki67$^+$ and (G) pSTAT5-expressing total and naive CD4$^+$ and CD8$^+$ T cells from spleens of aged μMT, aged WT, and young WT mice. (H) pγH2AX expression at baseline, in total and naive CD4$^+$ and CD8$^+$ T cells from spleens of aged μMT and WT mice. (**I**) Frequencies of Nur77$^+$ (left), Ki67$^+$ (middle), and CD69$^+$ CD25$^+$ (right) CD4$^+$ T cells upon in vitro stimulation of naive T cells (n = 9 to 12 per group). (**J** to **L**) (J) iAge index values, (K) SenMayo scores, and (L) trajectory analyses of bulk splenic CD3$^+$ cells from aged μMT and WT mice (n = 2 pooled cohoused mice per group). All experiments were repeated at least twice except for (C), (D), (H), and (J) to (L), which were obtained via a single experiment. Statistical difference between two means was determined via a Mann-Whitney test. Welch two-sample t test was used to assess the distributions of iAge index and SenMayo cell scores between WT and μMT. Data are means ± SEM. *P < 0.05, **P < 0.01, and ***P < 0.001. DN, CD4 CD8 double negative; SP, single positive; DP, CD4 CD8 double positive; MFI, mean fluorescence intensity.

cluster level, many of these differences were observed among individual clusters (fig. S4A), suggesting that B cells can broadly modulate the inflammatory and age-related profile of T cell subsets, with differences not associated with shifting cell proportions. Gene set enrichment analysis (GSEA) linked pathway analysis suggested that WT T cells display higher expression of pathways linked with proinflammatory cytokine signaling, T cell activation, and increased metabolic output, which was also observed at the individual cluster level (Fig. 2D).

Given these age-resistant changes in T cell gene expression from aged μMT mice, we also assessed T cell functional capacity. Ex vivo stimulation of T cells from μMT mice, via a PMA (phorbol 12-myristate 13-acetate)/ionomycin cocktail, confirmed their decreased inflammatory potential, given that CD8 T cells displayed reduced interferon-γ (IFN-γ) production and CD4 T cells produced limited IFN-γ and interleukin-17 (IL-17) compared with WT controls (Fig. 2E and fig. S4B). Furthermore, in the absence of stimulation, old μMT mice had fewer proliferating $Ki67^+$ CD4 T cells (Fig. 2F), as well as reduced expression of phosphorylated signal transducer and activator of transcription 5 (pSTAT5) and γH2AX, in total and naive T cells compared with WT controls (Fig. 2, G and H). These findings suggest reduced cytokine-mediated modulation, baseline cellular proliferation, and DNA damage in T cells from μMT mice, features which are thought to drive T cell dysfunction with age (*11*, *33*, *34*). We next directly assessed the functionality of naive T cells from aged μMT mice. Upon in vitro stimulation via plate-bound anti-CD3/CD28, purified naive T cells from aged μMT mice displayed increased frequencies of $Nur77^+$, $Ki67^+$, and $CD69^+$ $CD25^+$ cells compared with aged WT controls (Fig. 2I and fig. S4C). Across most markers, levels were comparable to responses of young T cells, suggesting a functionally younger phenotype of old μMT T cells after ex vivo stimulation.

Additional transcriptomic analyses confirmed that T cells from aged μMT mice scored lower iAge index (Fig. 2J and fig. S5A) and SenMayo scores (Fig. 2K and fig. S5B), which are algorithms that allow for assessment of inflammatory age (*35*) and senescence-associated features (*36*). Furthermore, pseudotime trajectory analyses highlighted differences in putative fates and branching nodes in splenic T cells from aged WT and μMT mice (Fig. 2L and fig. S5C), suggesting that in the absence of B cells, T cells fail to undergo activation and differentiation patterns occurring in WT T cells with age. Our findings indicate that, compared with WT mice, aged μMT mice harbor more naive T cells that are less activated at baseline and further retain the ability to undergo stronger responses upon activation, analogous to T cells from young WT mice.

B cell–deficient mice have improved health span and life span

Given that aged μMT mice harbor T cells that fail to adopt an immunosenescent phenotype, we next determined whether B cell deficiency could be associated with improvements in age-related parameters of frailty and metabolic dysfunction. Compared with WT controls, aged μMT mice had a slightly lower body weight yet displayed no overt differences in organ and tissue weights at 24 months old (fig. S6, A and B). However, B cell deficiency was linked with improvements in a 31-index frailty score (Fig. 3A and fig. S6C), a gold standard readout of mammalian health-span parameters (*37*), as well as improved metabolic sensitivity, as determined via glucose and insulin tolerance tests (GTTs and ITTs; Fig. 3B). μMT mice also demonstrated a pronounced increase in overall life span (median life-span increase of 36.3%), with some mice living longer than 3 years of age (Fig. 3C).

These improvements were further associated with decreased expression of various senescence-associated secretory phenotype (SASP), senescence, and fibrosis genes in the aging liver, lung, and muscle (Fig. 3, D and E, and fig. S6, D to F) and increased grip strength (Fig. 3F). In addition, changes in the T cell compartment of aged μMT mice were also observed in the blood, liver, and lung (Fig. 3, G and H, and fig. S7), suggesting that the global absence of B cells could prevent aspects of systemic aging of the T cell compartment in multiple tissues. However, limited differences were observed in the abundances of various circulating serum cytokines (fig. S6G), suggesting that improvements in inflammatory processes may be tissue specific. In line with decreased inflammatory SASP output in tissues, histological assessment confirmed notable improvements in tissue fibrosis and quadricep fiber area in aged μMT mice compared with WT controls (Fig. 3, I and J, and fig. S6, H and I). Cumulatively, these results suggest that an absence of B cells during the aging process is linked with a less immunosenescent T cell compartment, along with improvements in various parameters of age-associated decline in health-span parameters.

Aged B cells stimulate T cell immunosenescence

We next sought to determine whether depletion of B cells in middle-aged mice can prevent age-related T cell dysfunction. WT mice, 14 to 15 months old, were injected with a depleting anti-CD20 monoclonal antibody (CD20 mAb) or an isotype control (ISO) once every 2 weeks for 12 weeks (fig. S8A). As expected, upon completion of the 12-week loss-of-function treatment regimen, the spleen displayed a marked reduction in the relative abundance and cellularity of B cells and major B cell subsets (Fig. 4A and fig. S8, B to D). Although CD20 mAb treatment increased splenic T cell relative abundance, their cellularity remained unchanged (fig. S8E). Furthermore, treatment was associated with a mild increase in the CD4 T cell fraction, whereas CD8 T cells remained unchanged (fig. S8F).

Mice treated with CD20 mAb displayed an increased relative abundance of naive T cells and reductions of T_{EM} cells in both CD4 and CD8 compartments compared with ISO-treated controls (Fig. 4B and fig. S8G). Correspondingly, we observed a decrease in the relative abundance of splenic $PD1^+$ T cells and a trend toward a decrease in IFN-γ^+ T cells in CD20 mAb–treated mice (Fig. 4, C and D, and fig. S8, H and I). CD20 mAb treatment also decreased the expansion of T_{FH} cells with age (Fig. 4E), although T_{reg} cell frequency remained unchanged (fig. S8J). Similar observations regarding depletion of B2 cells and alterations to T cell heterogeneity were made in the blood (fig. S9, A to D), liver (fig. S9, E to H), and lung (fig. S9, I to L). Once again, these changes in the T cell compartment were observed in the absence of any changes in thymic size or thymocyte number, indicating that B cells use mechanisms independent of regulating thymocyte numbers to modulate the T cell compartment with age (fig. S9M).

CD20 mAb treatment in aged mice has previously demonstrated therapeutic efficacy in preventing age-associated metabolic dysfunction, which is linked with adaptive immune cell activity (*38*). Consequently, we speculated that CD20 mAb–treated mice might also display improvements in the 31-index frailty score and health condition. CD20 mAb–treated mice had lower body weights, which was associated with reductions in the weights of the kidneys and heart (fig. S10A). Furthermore, there was a strong trend toward improved frailty outcomes

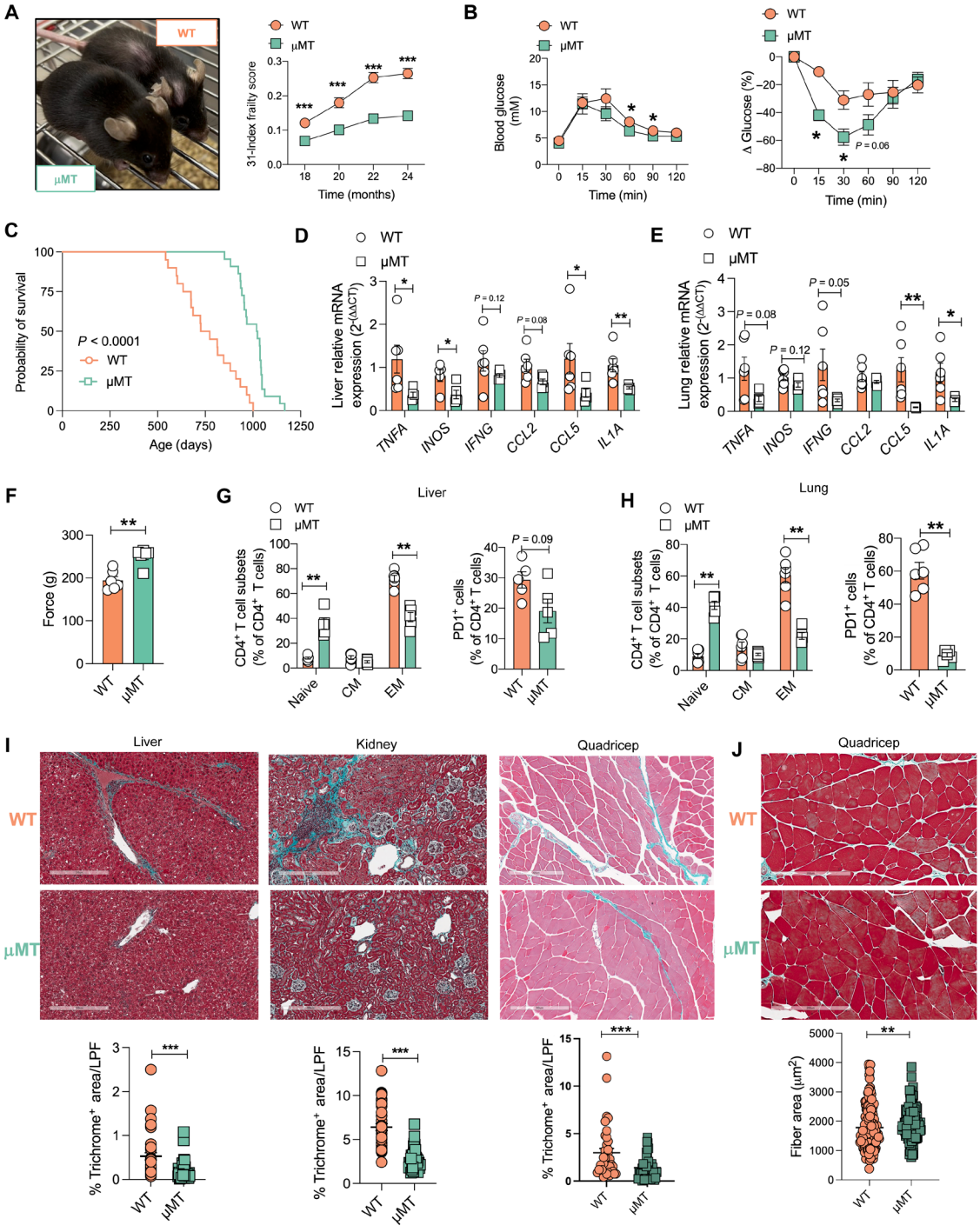

Fig. 3. B cell deficiency improves age-related health parameters. (**A**) Representative image (left) and 31-index frailty scores (right) from aged µMT and WT mice ($n = 9$ to 14 per group). (**B**) GTT (left) and ITT (right) results from aged µMT and WT mice ($n = 4$ to 5 per group). (**C**) Survival curves from aged µMT and WT mice ($n = 20$ to 22 per group). (**D**) qPCR gene expression of SASP markers in livers in aged µMT and WT mice ($n = 5$ or 6 per group). (**E**) qPCR gene expression of SASP markers in lungs in aged µMT and WT mice ($n = 4$ to 6 per group). (**F**) Grip strength analysis in aged µMT and WT mice ($n = 6$ per group). (**G**) Relative abundances of naive T cells, T_{EM} cells, and T_{CM} cells (left) and $PD1^+$ cells (right) among $CD4^+$ T cells in perfused livers of aged µMT and WT mice ($n = 5$ or 6 per group). (**H**) Relative abundances of naive T cells, T_{EM} cells, and T_{CM} cells (left) and $PD1^+$ cells (right) among $CD4^+$ T cells in perfused lungs of aged µMT and WT mice ($n = 5$ or 6 per group). (**I**) Representative images (top) and quantification (bottom) of tissue fibrosis via Masson's trichrome staining in livers, kidneys, and quadriceps from aged µMT and WT mice [$n = 39$ or 40 low-power fields (LPF) (tissue dependent) from four mice per group]. Scale bars, 300 µm. (**J**) Representative images (top) and quantification (bottom) of muscle fiber areas via Masson's trichrome staining in quadriceps from aged µMT and WT mice ($n = 160$ LPF from four mice per group. Scale bars, 200 µm. All experiments were repeated at least twice. Statistical difference between two means was determined via a Mann-Whitney test. Log-rank (Mantel-Cox) test was used for statistical analysis for survival curves. Data are means ± SEM. $^*P < 0.05$, $^{**}P < 0.01$, and $^{***}P < 0.001$.

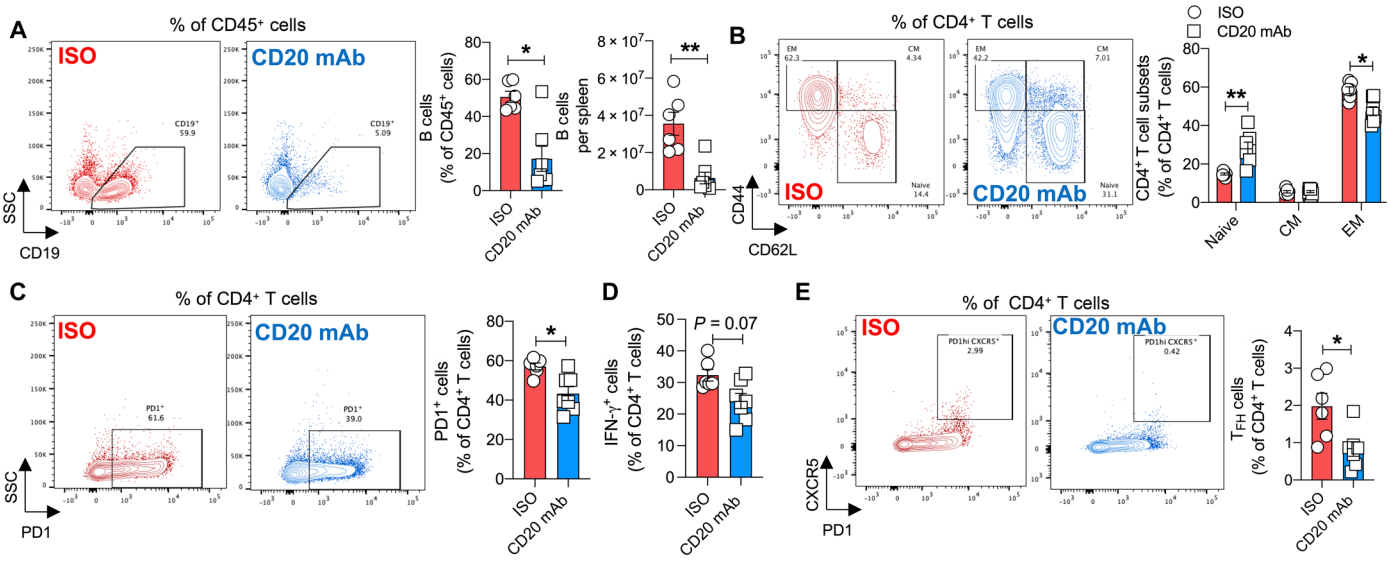

Fig. 4. B cell depletion with a CD20 mAb improves aging-associated CD4 T cell parameters. (**A** to **E**) Flow cytometric assessment of T cells from spleens of CD20 mAb– and ISO-treated aging mice ($n = 6$ or 7 per group). (A) Representative plots (left), relative abundances (middle), and cell numbers (right) of total B cells. (B) Representative plots (left) and relative abundances (right) of naive T cells, T_{EM} cells, and T_{CM} cells among $CD4^+$ T cells. (C) Representative plots (left) and relative abundances of $PD1^+$ cells among $CD4^+$ T cells. (D) Relative abundances of IFN-γ^+ cells among $CD4^+$ T cells after 5-hour ex vivo stimulation. (E) Representative plots (left) and relative abundances (right) of T_{FH} cells. All experiments were repeated at least twice. Statistical difference between two means was determined via a Mann-Whitney test. Data are means ± SEM. $^*P < 0.05$ and $^{**}P < 0.01$.

in CD20 mAb–treated mice compared with ISO controls (fig. S10B). These findings suggest that B cells can be actively targeted in late adulthood to prevent age-related decline in the naive T cell compartment and formation of T cell subsets linked with declining health span.

We next determined whether aged B cells could directly affect naive T cell activation compared with the effects of young B cells. We first isolated naive T cells from the spleens of young WT mice and cocultured them with B cells from either young or aged spleens, in the presence and absence of an anti-CD3 stimulant for 48 hours (fig. S11A). Coculture with B cells was able to increase the frequencies of $Nur77^+$, $Ki67^+$, $CD38^+$, and $PD1^+$ T cells, confirming that B cells can enhance T cell activation processes regardless of age (Fig. 5, A to D, and fig. S11, B to E). However, aged B cells displayed greater ability to reduce the frequency of naive T cells, which was more pronounced in the CD4 T cell compartment (Fig. 5E and fig. S11F). These results suggest that although B cells of any age can stimulate T cell activation, aged B cells have a superior ability to polarize CD4 T cells away from a naive phenotype in a coculture system.

We subsequently hypothesized that intravenous adoptive transfer of aged splenic B cells into young μMT recipient mice would acutely promote T cell activation and potentially alter some age-associated markers. μMT mice were selected as recipients because we reasoned that B cell deficiency would allow for transferred B2 cells to establish a niche in the spleen upon reconstitution. In line with previous B cell transfer strategies (*31*, *39*, *40*), we studied responses within 8 to 10 days (fig. S11G), given that previous studies have shown that aged immune cells can impart characteristics of tissue aging in as little as 7 days posttransfer (*34*). Eight to 10 days posttransfer, we observed successful reconstitution of young and aged B2 cells in the spleens of μMT recipient mice (Fig. 5F). Compared with recipients that received young B cells, recipients receiving aged B cells displayed an increase in the relative abundance of splenic T_{EM} cells, $PD1^+$ T cells, and T_{FH} cells, whereas T_{reg} cells and T_{CM} cells remained unchanged (Fig. 5, G to I, and fig. S11, H to L). Furthermore, in line with our in vitro experiments, transfer of aged B cells, compared with young B cells, only decreased the proportion of naive CD4 T cells in the spleen (Fig. 5G and fig. S11J). Cumulatively, these data suggest that although B cells have the ability to activate and differentiate T cells along the mouse life span, those situated in an aged spleen have a higher capacity for this effect, with a more pronounced effect on the CD4 T cell compartment.

B cell InsR signaling promotes age-related B cell phenotypes

We next sought to understand mechanisms that either fuel changes in the B cell phenotype with age or allow them to induce T cell dysfunction. Recent evidence suggests that aged B cells display a hypermetabolic profile linked with their proinflammatory capacity (*18*); however, the triggers that contribute to this process remain relatively unknown. The insulin signaling pathway downstream of the InsR is an evolutionarily conserved axis that boosts cellular metabolism and is negatively correlated with longevity across species (*41*). T cells have the InsR and up-regulate it upon activation to enhance inflammatory output during infection and autoimmunity (*42*). Given that aging is associated with hyperinsulinemia, elevated B cell metabolism, and increased B cell effector function, we investigated whether insulin signaling may serve as an environmental cue that harmonizes these observations to drive age-related B cell dysfunction and downstream T cell aging phenotypes.

To test this hypothesis, we first mined a public dataset comparing systemic young and aged B cells (*43*) and investigated whether insulin-related pathways were enriched among genes with higher expression in aged B cells. Aged B cells displayed an increased GeneRatio score in pathways related to the phosphatidyl inositol-kinase (PI3K)/protein

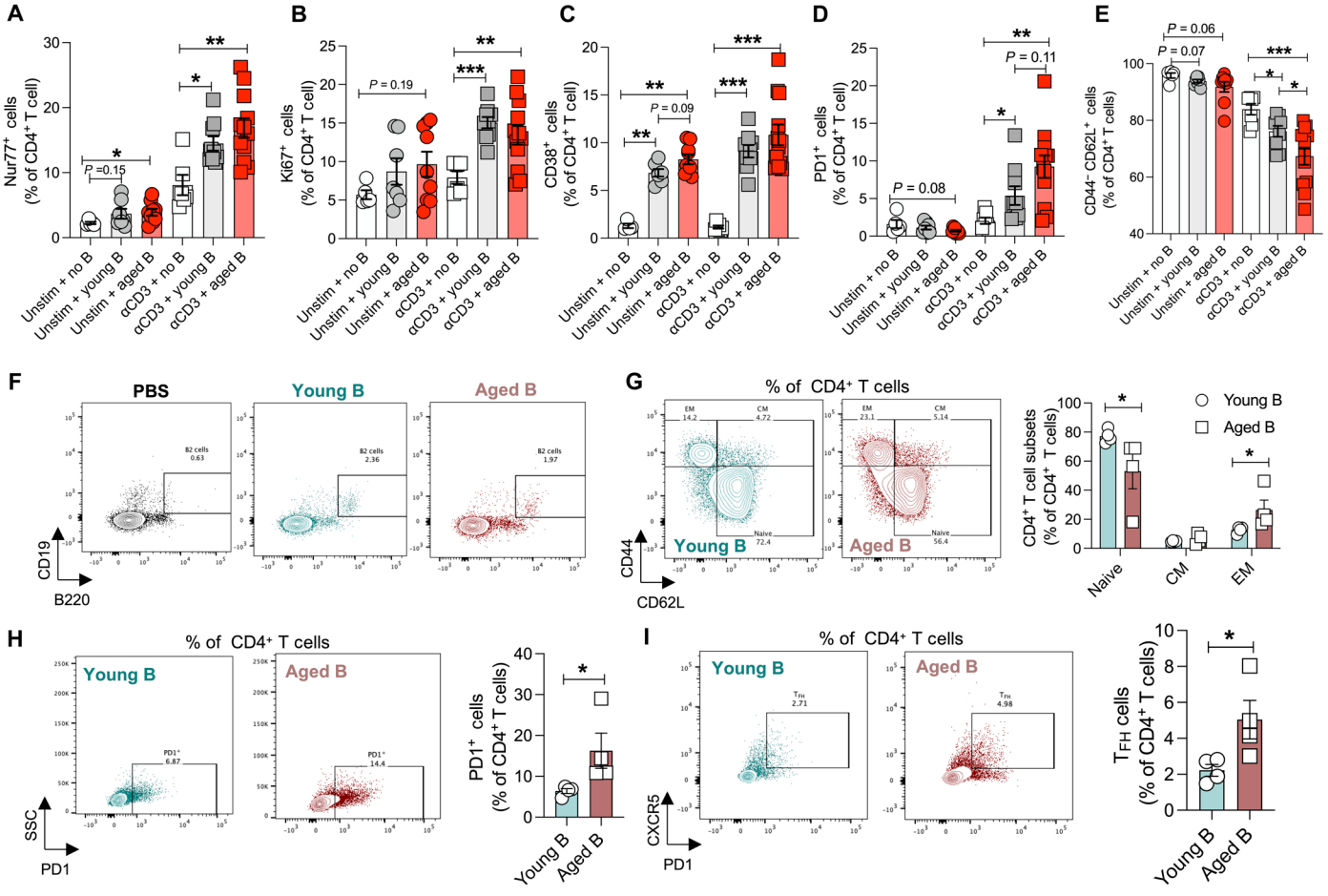

Fig. 5. Aged B cells have stronger capacity for altering the CD4 T cell compartment. (**A** to **E**) Flow cytometric assessment of splenic T cells after B cell and naive T cell coculture experiment in the presence and absence of an anti-CD3 stimulant for 48 hours ($n = 4$ to 12 per group). (A) Frequency of Nur77$^+$ cells among CD4$^+$ T cells. (B) Frequency of Ki67$^+$ cells among CD4$^+$ T cells. (C) Frequency of CD38$^+$ cells among CD4$^+$ T cells. (D) Frequency of PD1$^+$ cells among CD4$^+$ T cells. (E) Frequency of CD44$^-$ CD62L$^+$ cells among CD4$^+$ T cells. (**F** to **I**) Flow cytometric assessment of splenic T cells from recipient young μMT mice after transfer with aged B cells or young B cells ($n = 4$ per group). (F) Representative flow cytometry plots showing reconstitution of CD19$^+$ B220^{hi} B2 cells. (G) Representative plots (left) and relative abundances (right) of naive T cells, T_{EM} cells, and T_{CM} cells among CD4$^+$ T cells. (H) Representative plots (left) and relative abundances (right) of PD1$^+$ cells among CD4$^+$ T cells. (I) Representative plots (left) and relative abundances (right) of T_{FH} cells. All experiments were repeated at least twice. Statistical difference between two means was determined via a Mann-Whitney test. Data are means ± SEM. *$P < 0.05$, **$P < 0.01$, and ***$P < 0.001$.

kinase B (AKT) signaling axis driving the activation of the mammalian target of rapamycin (mTOR; fig. S12A). Phosphorylation of AKT at sites Thr^{308} and Ser^{473} is a key event required for the activation of mTOR, resulting in a cascade of events necessary for metabolic reprogramming of B cells (*44*). B2 cells from aged spleens displayed greater basal phosphorylation at the Thr^{308} AKT site and a trend toward increase at the Ser^{473} site, compared with young B cells (fig. S12, B and C). In contrast with the FOB population, CD11c$^+$ T-bet$^+$ ABCs displayed elevated basal phosphorylation of AKT at both sites (fig. S12, D and E), potentially supporting their increased metabolic demands, in line with previous findings (*18*). The formation of CD11c$^+$ T-bet$^+$ B cells is believed to be dependent on multiple stimuli, including Toll-like receptor (TLR), B cell receptor (BCR), and IL-21/IFN-γ cytokine signals (*21*). In vitro stimulation of B cells with these stimuli (ABC stim) resulted in increased expression of the *Insr* (fig.S12F). Furthermore, supplementing ABC stim B cells with insulin marginally expanded in vitro generation of CD11c$^+$ T-bet$^+$ B cells and boosted their production of T cell–modulating proinflammatory cytokines IFN-γ, tumor necrosis factor–α (TNFα), and IL-2 (fig. S12, G and H). Thus, B cell activation and subsequent up-regulation of the InsR may reflect a greater need for insulin consumption, which acts via the Akt signaling pathway to promote the generation of CD11c$^+$ T-bet$^+$ ABCs.

To test the role of InsR signaling in age-related B cell dysfunction, we generated and aged mutant mice in which B cells specifically lacked the InsR (CD19 Cre$^{+/-}$ InsR$^{FL/FL}$; B-InsR^{FL} mice) and compared them with age-matched WT Cre controls (CD19 Cre$^{+/-}$ InsR$^{WT/WT}$; B-InsR^{WT} mice). We first examined the effects of B cell–specific InsR ablation on aged splenic T cells. Although the frequency and number of total T cells remained unchanged, we observed a decrease in the proportion of CD4 T cells and an increased proportion of CD8 T cells in aged B-InsR^{FL} mice (fig. S13, A and B). In both the CD4 and CD8 T cell compartments, we observed an increased proportion of naive T cells and a reduction in the proportion of T_{EM} cells in the spleens of aged B-InsR^{FL} mice (Fig. 6A and fig. S13C). These findings were further accompanied

by a decrease in the frequency of PD1$^+$ T cells (Fig. 6B and fig. S13D) and a trend toward decreased IFN-γ$^+$ T cells and T_{FH} cells in the spleen, whereas T_{reg} cells remained unchanged (fig. S13, E and F). Similar changes in memory and naive T cells were observed among hepatic T cell subsets and lung CD8 T cells in aged B-InsR^{FL} mice (fig. S13, G to L), and these findings were once more observed to be independent of any changes in thymic involution or thymocyte number (fig. S13M).

We next assessed parameters of age-related decline in aged B-InsR^{FL} mice compared with B-InsR^{WT} controls. Despite no changes in body or organ weights (fig. S14, A and B), aged B-InsR^{FL} mice displayed improvements in 31-index frailty scoring (Fig. 6C and

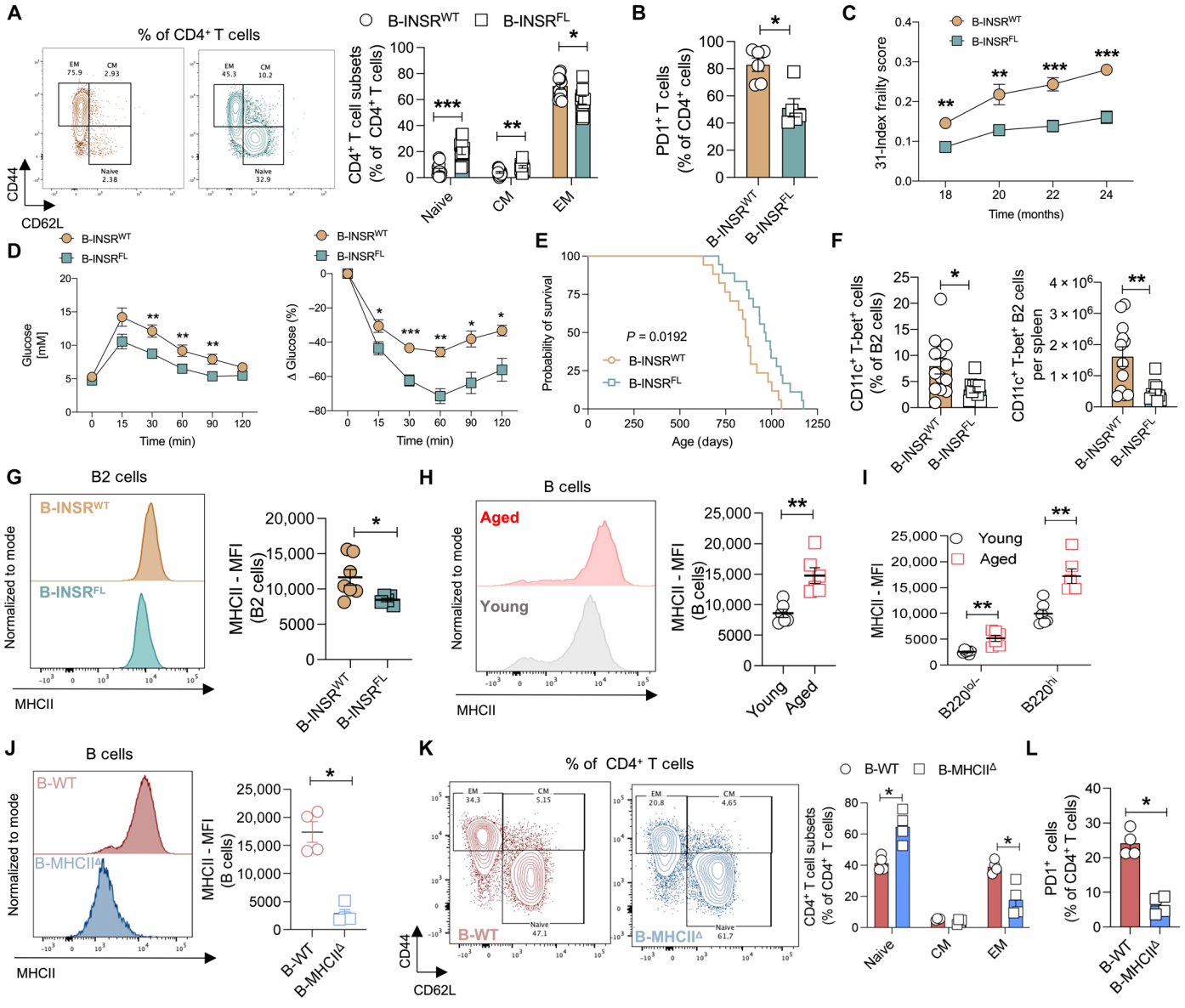

Fig. 6. B cell–intrinsic InsR and MHCII-mediated antigen presentation contributes to the aging of the CD4 T cell compartment. (**A** and **B**) Flow cytometric assessment of T cells from spleens of aged B-InsR^{FL} and B-InsR^{WT} mice ($n = 10$ to 13 per group). (A) Representative plots (left) and relative abundances (right) of naive T cells, T_{CM} cells, and T_{EM} cells among CD4$^+$ T cells. (B) Relative abundances of PD1$^+$ cells among CD4$^+$ T cells. (**C**) 31-Index frailty scores over time of aged B-InsR^{FL} and B-InsR^{WT} mice ($n = 8$ to 14 per group). (**D**) GTT (left) and ITT (right) results of aged B-InsR^{FL} and B-InsR^{WT} mice ($n = 6$ to 10 per group). (**E**) Survival curves from aged B-InsR^{FL} and B-InsR^{WT} mice ($n = 17$ or 18). (**F** and **G**) Flow cytometric assessment of B cells from spleens of aged B-InsR^{FL} and B-InsR^{WT} mice ($n = 5$ to 13 per group). (F) Relative abundances (left) and cell numbers (right) of CD11c$^+$ T-bet$^+$ B2 cells. (G) Representative plots (left) and MFIs (right) of MHCII in B2 cells. (**H** and **I**) Flow cytometric assessment of B cells in young and aged splenic cells ($n = 6$ per group). (H) Representative plots (left) and MFIs (right) of MHCII in total B cells. (I) MFIs of MHCII in B1 and B2 cell subsets. (**J** to **L**) Flow cytometric assessment of splenic B and T cells of chimeric mice containing 80%:20% ratios of either μMT bone marrow + MHC-II$^{-/-}$ bone marrow (B-MHCII^{Δ} mice) or μMT bone marrow + WT bone marrow (B-WT mice) ($n = 4$ per group). (J) Representative plots (left) and MFIs (right) of MHCII in total B cells. (K) Representative plots (left) and relative abundances (right) of naive T cells, T_{EM} cells, and T_{CM} cells among CD4$^+$ T cells. (L) Relative abundances of PD1$^+$ cells among CD4$^+$ T cells. Data are means ± SEM. All experiments were repeated at least twice. Statistical difference between two means was determined via a Mann-Whitney test. Log-rank (Mantel-Cox) test was used for statistical analysis for survival curves. *$P < 0.05$, **$P < 0.01$, and ***$P < 0.001$.

fig. S14E), glucose and insulin tolerance (Fig. 6D), grip strength (fig. S14C), and hepatic *Cdkn2a* and *Inos* expression (fig. S14D), as well as an increase in longevity (Fig. 6E), findings that are in line with a restored adaptive immune compartment (*45*).

To better understand how the InsR controls the aged B cell compartment, we surveyed the effects of InsR ablation on aged splenic B cell subsets and found no alterations to total B cell frequency and cellularity (fig. S15A). However, in the B cell compartment, we observed a marginal decrease in the proportion of B2 cells concomitant with an increase in the proportion of $B220^{lo/-}$ cells (fig. S15B). InsR-deficient B2 cells failed to express typical levels of CD23 (fig. S15C), expression of which has also been linked with the ability to activate T cells (*46*, *47*). Although we were therefore unable to define aged B2 cell subsets on the basis of expression of CD21 and CD23 (fig. S15D), we observed a marked decrease in the proportions and cellularity of $CD11c^+$ $T\text{-}bet^+$ B2 cells in $B\text{-}InsR^{FL}$ mice compared with $B\text{-}InsR^{WT}$ controls (Fig. 6F). Furthermore, class switch recombination subsets remained unchanged in InsR-deficient B2 cells at baseline (fig. S15E). We observed a decrease in MHCII expression (Fig. 6G) in aged $B\text{-}InsR^{FL}$ mice, suggesting a potential decline in their ability to stimulate CD4 T cells. Conversely, B2 cells from $B\text{-}InsR^{FL}$ mice showed no difference in MHCI levels compared to controls (fig. S15F), indicating that additional mechanisms may be involved in modulation of the CD8 T cell compartment.

B cells modulate age-related CD4 T cell compositional changes via MHCII

To assess whether lower levels of MHCII observed in $B\text{-}InsR^{FL}$ mice could contribute to T cell aging phenotypes, we first examined MHCII expression in WT mice. Compared with young B cells, aged WT B cells displayed increased up-regulation of pathways and machinery related to T cell activation and antigen presentation (Fig. 6, H and I, and fig. S16, A to D). Aged B2 cells in particular displayed a marked increase in MHCII expression (Fig. 6I). To directly test whether expression of MHCII could be one mechanism by which InsR action on B cells altered the T cell compartment during aging, we used a mixed bone marrow chimera strategy to generate mice in which B cells lacked expression of MHCII ($B\text{-}MHCII^{\Delta}$ mice). Briefly, 11-month recipient mice were irradiated and subsequently reconstituted with bone marrow containing 4:1 ratios of μMT bone marrow and either $MHCII^{-/-}$ ($B\text{-}MHCII^{\Delta}$) or WT bone marrow ($B\text{-}MHCII^{WT}$). At 3 to 4 months postreconstitution, overall splenic B cell proportion and cellularity remained unchanged, but B cells from $B\text{-}MHCII^{\Delta}$ mice displayed a substantial loss in MHCII expression (Fig. 6J and fig. S17, A to C). Loss of B cell–specific MHCII was associated with a decrease in the frequencies of ABCs, IgM^+ IgD^-, and IgM^- IgD^- B cells, as well as a decrease in the proportion and cellularity of $CD11c^+$ $T\text{-}bet^+$ B2 cells (fig. S17, D to F).

Although the proportion of total T cells remained unchanged, $B\text{-}MHCII^{\Delta}$ mice displayed a decrease in overall T cell cellularity (fig. S17, G and H). Further evaluation of the splenic CD4 T cell compartment unveiled an increase in proportion of naive CD4 T cells and a decrease in the proportions of T_{EM} and $PD1^+$ T cells in $B\text{-}MHCII^{\Delta}$ compared with $B\text{-}MHCII^{WT}$ mice (Fig. 6, K to L). $B\text{-}MHCII^{\Delta}$ mice also displayed a decrease in the proportion of T_{FH} cells (fig. S17, I and J). In the CD8 T cell compartment, only a decrease in T_{CM} cells was observed, whereas naive, T_{EM}, and $PD1^+$ cells remained unchanged, suggesting that B cell–mediated changes in CD8 T cells may occur in part independently of alterations to the CD4 T cell compartment (fig. S17, K to L). Overall, these data suggest that B cell–associated MHCII, which is induced by InsR signaling across the mouse life span, is a key factor that can drive compositional and phenotypical changes in CD4 T cells with age.

DISCUSSION

Existing models of T cell immunosenescence speculate that age-associated thymic involution results in decreased generation of naive T cells, which are subsequently forced to undergo epigenomic alterations to sustain their numbers in the periphery, yet consequently develop maladaptations linked with increased inflammatory change and susceptibility toward terminal differentiation (*8*, *11*, *12*). Accordingly, an aged T cell compartment displays an overabundance of expanded memory, senescent-like, and exhausted T cell subsets associated with clonal restriction. However, this differentiation from a naive state appears to be directly influenced by cellular and secreted mediators present in the aged environment, although their identities remain largely unknown (*43*). Here, through various methods of B cell manipulation, we show that B cells are one such cell type that contributes to this differentiation process. Mice lacking B cells displayed an increase in naive T cell abundance and a decrease in various differentiated T cell subsets into old age.

Transcriptionally, T cells isolated from aged B cell–deficient mice displayed a reduction in mediators and intercellular pathways regulating these processes and had a diverse TCR that resisted clonal restriction. Naive T cells from B cell–deficient mice also displayed decreased expression of pSTAT5, signaling through which has been documented to drive intrinsic changes in aged naive CD4 T cells at the epigenomic level (*11*), and displayed strong activation responses upon in vitro stimulation, an ability typically lost with age (*48*). These findings suggest that a lack of B cells across the life span may shield naive T cells from undergoing signaling linked to immunosenescence. Adoptive transfer of aged B cells in vivo or coculture with naive T cells in vitro was found to skew CD4 T cells away from naive states. These findings cumulatively suggest that instead of an expansion of naive T cells in B cell–deficient mice, their increase in abundance is likely linked with increased quiescence and decreased activation.

Accordingly, our models of B cell deficiency demonstrate that B cells can influence overall decline in health-span parameters with age. Aged B cell–deficient mice displayed improvements in metabolic parameters, senescence, fibrosis, frailty, and life span. CD20 mAb therapy has previously been demonstrated to confer metabolic improvements in aged mice, notably by restoring glucose homeostasis, insulin sensitivity, and adipose tissue lipolysis (*38*, *49*). In addition, immunoglobulin G (IgG) may function as an aging factor that promotes adipose tissue dysfunction and metabolic decline (*50*, *51*). Here, we expand upon the potential mode of action of CD20 mAb therapy and demonstrate that targeted depletion of B cells, given in late adulthood in mice, can slow aging of the systemic T cell compartment, most notably preventing the formation of T_{EM} cells and conserving the naive T cell pool. However, it is important to note that CD20 mAb treatment does not deplete terminally differentiated antibody-secreting cells, which accumulate with age and produce proinflammatory cytokines, particularly in the bone marrow (*20*, *52*). In addition, the bone marrow is a niche for memory T cell survival and quiescence (*53*, *54*), and it remains to be determined whether B cell depletion therapies can also modulate this pool of T cells.

Evaluation of mechanisms that define aging features in the B cell compartment led us to identify B cell–specific InsR signaling as an environmental trigger. Ablation of B cell–specific InsR in aged mice resulted in changes in the relative abundances of various B cell subsets, a reduction in CD11c$^+$ T-bet$^+$ B cells, and a T cell compartment that resisted alterations in composition typically observed in aged conditions, concurrent with improvements in longevity and health-span parameters. CD11c$^+$ T-bet$^+$ B cells have previously been demonstrated to form from nucleic acid sensing via TLR7/9, ligation of the BCR, IL-21, and IFN-γ cytokine signaling (*21*, *22*). Here, we identify InsR signaling as an additional environmental trigger that supports the formation of CD11c$^+$ T-bet$^+$ B cells. Given that ABCs have greater metabolic needs, it seems likely that InsR signaling facilitates metabolic processes, such as glycolysis, to support their expansion and proinflammatory cytokine output. Consistently, in T cells, InsR signaling promotes T cell inflammatory output by boosting their cellular metabolism (*55*).

We found that an absence of B cells or deletion of their InsR resulted in a decline in IFN-γ$^+$ T cells, as well as IL-21–secreting PD1$^+$ CD4 T cells, suggesting that the presence of aged B cells likely forms a positive feedback loop whereby T cell–derived cytokines such as IL-21 and IFN-γ continue to support CD11c$^+$ T-bet$^+$ B cell expansion in congruence with TLR7/9, BCR, and InsR signals. Similar B–CD4 T cell circuits govern instances of humoral responses (*56*). In line with this idea, lack of MHCII expression in B cells decreased the relative abundance of PD1$^+$ CD4 T cells with age and additionally limited the expansion of CD11c$^+$ T-bet$^+$ and class-switched IgM$^-$ IgD$^-$ B2 cells. Improvements in age-associated metabolic disease parameters were also observed in mice in which T_{reg} cells specifically lacked the InsR (*57*), positing that insulin signaling may exert its anti-longevity effects via multiple immune cells.

Aged B cells display increased expression of antigen-presenting molecules, costimulatory molecules, and associated signaling pathways. Specific ablation of MHCII from B cells shielded the CD4 T cell compartment from age-associated phenotypic and compositional changes, and our findings suggest the presence of an InsR–B cell–MHCII axis involved in directly evoking CD4 T cell immunosenescence. Although B cells could exert influence on both CD4 and CD8 T cells in our μMT, anti-CD20 mAb, and B-InsR^{FL} models, more work is needed to understand how B cells drive compositional changes in the CD8 T cell compartment. In both our in vitro and in vivo gain-of-function experiments, aged B cells primarily skewed CD4 T cells away from a naive state. Furthermore, B-InsR^{FL} mice did not display a similar decline in expression of B cell MHCI, and hence, these mechanisms promoting CD8 T cell immunosenescence may potentially occur also through indirect mechanisms, such as communication with another cell type, or production of secretory mediators, such as antibodies or cytokines (*31*, *58*).

Collectively, our results support a model where intrinsic age-associated environmental triggers, including InsR signaling, contribute to aging features of the B cell compartment. Aging B cells thereby contribute to T cell immunosenescence, which results in part from T cell activation and proliferative stress, ultimately leading to loss of the naive T cell pool and TCR diversity and fueling the formation of a clonally restricted, inflammatory T cell compartment during aging. For CD4 T cells specifically, this process is influenced by B cell MHCII expression, which is modulated by B cell–specific InsR signaling across the life span. These results place nutrient sensing by B cells and intercellular communication between B and T cells as key orchestrators of adaptive immune system aging, with the capacity to influence health span and longevity.

MATERIALS AND METHODS

Study design

The aim of the study was to investigate B cells in age-associated adaptive immune dysfunction and in health-span and life-span parameters. We used mouse models of B cell depletion, such as mice lacking a membrane-bound IgM displaying a B cell developmental arrest (μMT mice) and pharmacological depletion of B cells using anti-CD20 mAb, to study the role of B cells on CD4 T cell immunosenescence and aging parameters. We also used mouse models with B cell–specific InsR ablation and mixed bone marrow chimeric mice in which B cells lacked expression of MHCII to understand mechanisms by which aging affects B cells that in turn affects T cells. Using flow cytometry, single-cell RNA sequencing, in vitro and ex vivo cultures, gene expression assays, and enzyme-linked immunosorbent assay, we demonstrated a role for B cells in age-related reduction of naive CD4 T cells and associated differentiation toward immunosenescent T cell subsets and clonal restriction of TCR. With histology, physiological tests (e.g., metabolic tolerance tests and grip strength analysis), and a 31-point frailty index, we also assessed health span and life span in mouse models. All the experimental procedures were performed under the approval of Animal User Protocols by the Animal Care Committee at the University Health Network. Please see the Supplementary Materials for additional details on study design.

Mice

C57BL/6J (000664), CD19-cre (006785), Insr$^{fl/fl}$ (006955), μMT mice (002288), and MHCII$^{-/-}$ mice (003584) were purchased from the Jackson Laboratory. CD19 cre$^{+/-}$ Insr$^{fl/fl}$ mice were generated in-house by intercrossing CD19-cre mice with Insr$^{fl/fl}$ mice. Mice were maintained in a pathogen-free, temperature-controlled, and 12-hour light and dark cycle environment at the Toronto Medical Discovery Tower animal research facility. Female mice were used for experiments, unless otherwise specified. In-house generated mice from multiple litters and cages were used and randomized to experimental groups.

Immune cell isolation

Mice were euthanized using CO_2 fixation before collecting organs, blood, and lymphoid organs. Spleens were processed into single-cell suspensions and filtered through a 40-μm cell strainer followed by hemolysis. Blood was collected in heparin (1000 U/ml, BioShop) by cardiac puncture after euthanasia or saphenous vein from live mouse and subjected to hemolysis for single-cell suspension. Thymuses were processed into single-cell suspensions and filtered through a 40-μm cell strainer without hemolysis. Livers were perfused and dissociated using gentleMACS Dissociator (Miltenyi Biotec), as previously described (*59*). Lungs were perfused and digested with collagenase IV (1 mg/ml, Sigma-Aldrich) for 1 hour at 37°C. Single-cell suspensions were isolated from lung and liver using Percoll density gradient centrifugation followed by hemolysis.

Flow cytometry

Single-cell suspensions from different mouse organs and blood were stained with Zombie ultraviolet dye (BioLegend) for viability at room

temperature for 20 min followed by Fc blocking with CD16/32 (93, BioLegend) at 4°C for 20 min. For staining of intracellular cytokines, single-cell suspensions were stimulated with phorbol myristate acetate in the presence of Golgi Stop (eBioscience) for 5 hours before surface staining. The cells were further stained with fluorophore-conjugated antibodies (table S2) for 30 min at 4°C in dark. Intracellular staining for most targets (table S2) was done for 45 min at room temperature (RT) in the dark after fixation and permeabilization using Foxp3 staining buffer set (eBioscience). Phosphoflow for pAKT staining was performed as previously described (*60*). Briefly, cells were stained with Zombie ultraviolet dye (BioLegend) for viability at room temperature for 2 min followed by Fc blocking with CD16/32 (93, BioLegend) at 4°C for 2 min. Surface markers were stained for 7 min at 4°C. Intracellular staining was done for pAKT-Ser473 (SDRNR, Invitrogen) and pAKT-pT308 (J1-223.371, BD Biosciences) for 45 min at RT in the dark after fixation and permeabilization overnight at 4°C using Foxp3 staining buffer set (eBioscience). The antibody concentrations were used according to the manufacturer's recommendations. Cells were analyzed on LSR-Fortessa X-20 at the Princess Margaret Hospital Flow Cytometry Facility, University Health Network (Toronto, Canada). All the raw data for flow cytometry were analyzed using FlowJo (v.10.7.1).

Gene expression assays

Total RNA was extracted from flash frozen cell pellets and organs using the RNeasy Mini Kit (QIAGEN). Reverse transcription was performed using the SensiFAST cDNA Synthesis Kit (Bioline). Quantitative polymerase chain reaction (qPCR) was performed on a QuantStudio 6 Flex Real-Time PCR system (Thermo Fisher Scientific) using SYBR Green Master Mix reagent (Applied Biosystems). Samples were normalized to housekeeping genes *HPRT*, *GAPDH*, *B2M*, or *ACTB*. Relative changes in gene expression were calculated on the basis of the ΔΔCT method using the equation $2^{-\Delta\Delta CT}$. Fold changes were presented in comparison with the control groups. See table S1 for primer sequences.

Enzyme-linked immunosorbent assay and Luminex

Cytokine concentrations for IL-2, IFN-γ, and TNFα were measured in the supernatant using BioLegend kits following the manufacturer's protocol. Serum samples were sent to Eve Technologies for Mouse Cytokine/Chemokine 32-Plex Discovery Assay Array (MD32).

In vitro ABC generation

Spleens were processed into single-cell suspensions and filtered through a 40-μm cell strainer. B cells were purified from single-cell suspensions using the Pan B cell Isolation kit II (Miltenyi Biotec), and 200,000 cells per well were plated in a 96-well, U-bottom plate (Falcon) cultured in 200 μl RPMI 1640 (Wisent) supplemented with penicillin (100 U/ml, Sigma-Aldrich), streptomycin (100 mg/ml, Sigma-Aldrich), L-glutamine (2 mM, Sigma-Aldrich), 2-mercaptoethanol (50 mM, Sigma-Aldrich), and 10% heat-inactivated fetal bovine serum (FBS; Wisent) with or without the following: R848 (500 ng/ml, Miltenyi Biotec), anti-mouse IgM $F(ab')_2$ fragment (1 μg/ml, BioLegend), IL-21 (50 ng/ml, BioLegend), and insulin (100 ng/ml). B cells were cultured for 48 hours before collection of the supernatant and cell pellet.

In vitro T cell culture assays

T cells and B cells were processed by negative selection magnetic bead separation from spleens of young and old mice for coculture as described in the Supplementary Materials. Naive T cells purified from spleens were assessed for in vitro functional assays as described in the Supplementary Materials.

Bone marrow chimeras

Eleven-month-old WT mice were irradiated with 950 cGy using a Cesium-137 irradiator (Gammacell 40 Exactor) and reconstituted with intravenous injections of 6,000,000 bone marrow cells. The following mixtures were obtained using 4- to 5-month-old donor mice: B-MHCII$^{\Delta}$ mice (80% μMT and 20% MHCII$^{-/-}$) and B-WT mice (80% μMT and 20% WT). Bone marrow cells were obtained by flushing mouse femurs and tibias with phosphate-buffered saline (PBS) using a 26-gauge needle, dissociated into single-cell suspension, hemolyzed, washed in PBS, and counted. Bone marrow chimeric mice were treated with Baytril drinking water for 2 weeks after bone marrow cell transfer and aged for 3 to 4 months before sacrifice and immune cell assessment via flow cytometry.

Adoptive transfers

Young and aged B cells were purified from prepared WT splenocytes using the Pan B Cell Isolation Kit II (Miltenyi Biotec). Three-month-old μMT recipient mice received either donor 13 to 15 million B cells from young and aged WT mice. Recipient mice were euthanized 7 to 9 days postadoptive transfer for assessment of immune cell composition via flow cytometry.

Histology

Tissue histology and analysis on mouse tissues are described in the Supplementary Materials.

Anti-CD20 mAb treatment

Fourteen- to 15-month-old C57BL/6J mice were injected intraperitoneally with anti-CD20 mAb (300 μg, SA271G2, BioLegend) or rat IgG2b, ISO antibody (300 μg, RTK4530, BioLegend), once every 2 weeks for 12 weeks.

Metabolic tolerance tests

Metabolic tests were conducted as previously described (*61*). Mice were fasted overnight for GTTs and for 6 to 7 hours in the morning for ITTs. GTTs and ITTs were performed using 1.5 g of glucose per kg body mass and 0.5 U of human insulin per kg body mass via intraperitoneal injection. Blood glucose measurements were made at 0-, 15-, 30-, 60-, 90-, and 120-min time points with a glucometer (Contour next EZ).

Frailty scoring

Health span of mice was assessed using a 31-item frailty index to identify humane interventions and end points. The scoring was done every 2 months, starting at 18 months. The 31-item frailty index is a list of noninvasive clinical assessment of 31 potential deficits in aging mice that are scored 0, 0.5, or 1 based on the severity, which generates an average score for each mouse (*37*).

Grip strength assessment

Mouse grip strength was assessed using a grip strength test machine (Bioseb) following the manufacturer's instructions. Grip strength was quantified as an average of three individual measurements from each mouse.

T cell single-cell RNA and TCR sequencing analyses

Cell sorting and preparation

Cells from spleens of aged μMT and WT mice were prepared as described above. Cells were blocked with Fc block CD16/32 (93) and stained with viability dye zombie aqua, CD45 (30-F11), CD3 (17A2), and CD19 (6D5) (BioLegend), using methods described above for surface staining. Live $CD45^+$ $CD3^+$ $CD19^-$ cells were sorted using a MoFlo Astrios Sorting Machine, at the Princess Margaret Hospital Flow Cytometry Facility, University Health Network (Toronto, Canada), and collected into Eppendorf tubes containing a 500-μl cushion of RPMI 1640 (Wisent) with 10% heat-inactivated FBS (Wisent). Samples were processed according to protocols for 5′ v2 chemistry with VDJ (T) library enrichment from 10X Genomics at the Princess Margaret Genomics Centre and sequenced on a NovaSeq 6000 instrument. Postsequencing, to align read and generate feature barcode matrices, raw data were subjected to the Cell Ranger pipeline -6.1.2. Cell Ranger outputs indicated the following yields: WT $CD3^+$ cells: 8999 cells with 7405 cells with productive VJ spanning pairs and μMT $CD3^+$ cells: 8312 cells with 6268 cells with productive VJ spanning pairs.

TCR data integration and clonality analysis

To visualize the distribution of expanded T cell clones, the clonotype information from the 10× TCR sequencing analysis was merged with the final Seurat object metadata based on cell barcodes. This step linked each cell in the UMAP to its specific TCR clonotype ID. For the UMAP overlay plot, the size of each clonally expanded population (defined as clones with >2 cells) was represented by a circle. The position of this circle was determined by the average UMAP coordinate of all cells within that clone, and its size was scaled proportionally to the number of cells in the clone.

The Wilcoxon rank sum test and Kolmogorov-Smirnov test were used to assess whether the distributions of clonally expanded cell populations between the WT and μMT cell populations were significantly different. In both cases, the distributions were deemed significantly different with a very low P value ($P < 2.2 \times 10^{-16}$), with the WT cells exhibiting greater clonal expansion across larger numbers of unique TCR clones.

iAge index and SenMayo score calculation

The inflammatory aging (iAge) index was calculated by multiplying normalized and scaled gene expression with the corresponding coefficient of the gene in the iAge gene set (*35*). Cellular senescence was scored using the AddModuleScore function in Seurat with the SenMayo gene set (*36*, *62*, *63*). Gene names in the gene set were converted to their mouse homolog. The Welch two-sample t test was used to assess whether the distributions of cell scores between the WT and μMT cell populations were significantly different. In both cases, the distributions were deemed significantly different with a very low P value ($P < 2.2 \times 10^{-16}$). For details on processing, pathway analysis, and trajectory analysis, please refer to the Supplementary Materials.

Mined data analyses

Please see the Supplementary Materials for details on bioinformatics reanalysis of mouse young and aged B cell GeneRatio analyses (*43*).

Statistical analyses

Statistical difference between two means was determined via a Mann-Whitney test (i.e., did not assume normal distribution), with GraphPad Prism Software Inc. (v.9.0.0) unless otherwise indicated. All data are presented as means ± SEM. Statistical significance was set at $P < 0.05$. $^*P < 0.05$, $^{**}P < 0.01$, and $^{***}P < 0.001$.

Supplementary Materials

The PDF file includes:

Materials and Methods
Figs. S1 to S17
Tables S1 and S2
Legends for data files S1 to S3
References (*64*–*74*)

Other Supplementary Material for this manuscript includes the following:

Data files S1 to S3
MDAR Reproducibility Checklist

REFERENCES AND NOTES

1. T. Flatt, A new definition of aging? *Front. Genet.* **3**, 148 (2012).
2. B. K. Kennedy, S. L. Berger, A. Brunet, J. Campisi, A. M. Cuervo, E. S. Epel, C. Franceschi, G. J. Lithgow, R. I. Morimoto, J. E. Pessin, T. A. Rando, A. Richardson, E. E. Schadt, T. Wyss-Coray, F. Sierra, Geroscience: Linking aging to chronic disease. *Cell* **159**, 709–713 (2014).
3. E. L. Goldberg, V. D. Dixit, Drivers of age-related inflammation and strategies for healthspan extension. *Immunol. Rev.* **265**, 63–74 (2015).
4. C. Franceschi, P. Garagnani, P. Parini, C. Giuliani, A. Santoro, Inflammaging: A new immune-metabolic viewpoint for age-related diseases. *Nat. Rev. Endocrinol.* **14**, 576–590 (2018).
5. J. J. Baechle, N. Chen, P. Makhijani, S. Winer, D. Furman, D. A. Winer, Chronic inflammation and the hallmarks of aging. *Mol. Metab.* **74**, 101755 (2023).
6. J. Nikolich-Zugich, The twilight of immunity: Emerging concepts in aging of the immune system. *Nat. Immunol.* **19**, 10–19 (2018).
7. J. M. Bartleson, D. Radenkovic, A. J. Covarrubias, D. Furman, D. A. Winer, E. Verdin, SARS-CoV-2, COVID-19 and the ageing immune system. *Nat. Aging* **1**, 769–782 (2021).
8. J. J. Goronzy, C. M. Weyand, Mechanisms underlying T cell ageing. *Nat. Rev. Immunol.* **19**, 573–583 (2019).
9. M. Mittelbrunn, G. Kroemer, Hallmarks of T cell aging. *Nat. Immunol.* **22**, 687–698 (2021).
10. Q. Qi, D. W. Zhang, C. M. Weyand, J. J. Goronzy, Mechanisms shaping the naïve T cell repertoire in the elderly—Thymic involution or peripheral homeostatic proliferation? *Exp. Gerontol.* **54**, 71–74 (2014).
11. H. Zhang, R. R. Jadhav, W. Cao, I. N. Goronzy, T. V. Zhao, J. Jin, S. Ohtsuki, Z. Hu, J. Morales, W. J. Greenleaf, C. M. Weyand, J. J. Goronzy, Aging-associated HELIOS deficiency in naive $CD4^+$ T cells alters chromatin remodeling and promotes effector cell responses. *Nat. Immunol.* **24**, 96–109 (2023).
12. H. Zhang, H. Okuyama, A. Jain, R. R. Jadhav, B. Wu, I. Sturmlechner, J. Morales, S. Ohtsuki, C. M. Weyand, J. J. Goronzy, PREX1 improves homeostatic proliferation to maintain a naïve $CD4^+$ T cell compartment in older age. *JCI Insight* **9**, e172848 (2024).
13. W. Cao, I. Sturmlechner, H. Zhang, J. Jin, B. Hu, R. R. Jadhav, F. Fang, C. M. Weyand, J. J. Goronzy, TRIB2 safeguards naive T cell homeostasis during aging. *Cell Rep.* **42**, 112195 (2023).
14. G. Soto-Heredero, M. M. Gómez de Las Heras, J. I. Escrig-Larena, M. Mittelbrunn, Extremely differentiated T cell subsets contribute to tissue deterioration during aging. *Annu. Rev. Immunol.* **41**, 181–205 (2023).
15. S. Han, P. Georgiev, A. E. Ringel, A. H. Sharpe, M. C. Haigis, Age-associated remodeling of T cell immunity and metabolism. *Cell Metab.* **35**, 36–55 (2023).
16. B. Hu, R. R. Jadhav, C. E. Gustafson, S. L. Saux, Z. Ye, X. Li, L. Tian, C. M. Weyand, J. J. Goronzy, Distinct age-related epigenetic signatures in CD4 and CD8 T cells. *Front. Immunol.* **11**, 585168 (2020).
17. J. J. Goronzy, W. W. Lee, C. M. Weyand, Aging and T-cell diversity. *Exp. Gerontol.* **42**, 400–406 (2007).
18. D. Frasca, M. Romero, D. Garcia, A. Diaz, B. B. Blomberg, Hyper-metabolic B cells in the spleens of old mice make antibodies with autoimmune specificities. *Immun. Ageing* **18**, 9 (2021).
19. C. A. Siegrist, R. Aspinall, B-cell responses to vaccination at the extremes of age. *Nat. Rev. Immunol.* **9**, 185–194 (2009).
20. N. Schaum, B. Lehallier, O. Hahn, R. Pálovics, S. Hosseinzadeh, S. E. Lee, R. Sit, D. P. Lee, P. M. Losada, M. E. Zardeneta, T. Fehlmann, J. T. Webber, A. M. Geever, K. Calcuttawala, H. Zhang, D. Berdnik, V. Mathur, W. Tan, A. Zee, M. Tan, Tabula Muris Consortium, A. O. Pisco, J. Karkanias, N. F. Neff, A. Keller, S. Darmanis, S. R. Quake, T. Wyss-Coray, Ageing hallmarks exhibit organ-specific temporal signatures. *Nature* **583**, 596–602 (2020).
21. M. P. Cancro, Age-associated B cells. *Annu. Rev. Immunol.* **38**, 315–340 (2020).
22. D. Dai, S. Gu, X. Han, H. Ding, Y. Jiang, X. Zhang, C. Yao, S. Hong, J. Zhang, Y. Shen, G. Hou, B. Qu, H. Zhou, Y. Qin, Y. He, J. Ma, Z. Yin, Z. Ye, J. Qian, Q. Jiang, L. Wu, Q. Guo, S. Chen, C. Huang, L. C. Kottyan, M. T. Weirauch, C. G. Vinuesa, N. Shen, The transcription factor ZEB2 drives the formation of age-associated B cells. *Science* **383**, 413–421 (2024).
23. I. Rastogi, D. Jeon, J. E. Moseman, A. Muralidhar, H. K. Potluri, D. G. McNeel, Role of B cells as antigen presenting cells. *Front. Immunol.* **13**, 954936 (2022).

24. P. Shen, S. Fillatreau, Antibody-independent functions of B cells: A focus on cytokines. *Nat. Rev. Immunol.* **15**, 441–451 (2015).
25. J. K. Whitmire, M. S. Asano, S. M. Kaech, S. Sarkar, L. G. Hannum, M. J. Shlomchik, R. Ahmed, Requirement of B cells for generating $CD4^+$ T cell memory. *J. Immunol.* **182**, 1868–1876 (2009).
26. I. Misumi, J. K. Whitmire, B cell depletion curtails $CD4^+$ T cell memory and reduces protection against disseminating virus infection. *J. Immunol.* **192**, 1597–1608 (2014).
27. S. Hong, Z. Zhang, H. Liu, M. Tian, X. Zhu, Z. Zhang, W. Wang, X. Zhou, F. Zhang, Q. Ge, B. Zhu, H. Tang, Z. Hua, B. Hou, B cells are the dominant antigen-presenting cells that activate naive $CD4^+$ T cells upon immunization with a virus-derived nanoparticle antigen. *Immunity* **49**, 695–708.e4 (2018).
28. J. G. Cyster, C. D. C. Allen, B cell responses: Cell interaction dynamics and decisions. *Cell* **177**, 524–540 (2019).
29. L. N. Adler, W. Jiang, K. Bhamidipati, M. Millican, C. Macaubas, S.-C. Hung, E. D. Mellins, The other function: Class II-restricted antigen presentation by B cells. *Front. Immunol.* **8**, 319 (2017).
30. J. M. B. Prieto, M. J. B. Felippe, Development, phenotype, and function of non-conventional B cells. *Comp. Immunol. Microbiol. Infect. Dis.* **54**, 38–44 (2017).
31. D. A. Winer, S. Winer, L. Shen, P. P. Wadia, J. Yantha, G. Paltser, H. Tsui, P. Wu, M. G. Davidson, M. N. Alonso, H. X. Leong, A. Glassford, M. Caimol, J. A. Kenkel, T. F. Tedder, T. M. Laughlin, D. B. Miklos, H.-M. Dosch, E. G. Engleman, B cells promote insulin resistance through modulation of T cells and production of pathogenic IgG antibodies. *Nat. Med.* **17**, 610–617 (2011).
32. D. Kitamura, J. Roes, R. Kühn, K. Rajewsky, A B cell-deficient mouse by targeted disruption of the membrane exon of the immunoglobulin mu chain gene. *Nature* **350**, 423–426 (1991).
33. L. Kell, A. K. Simon, G. Alsaleh, L. S. Cox, The central role of DNA damage in immunosenescence. *Front. Aging* **4**, 1202152 (2023).
34. M. J. Yousefzadeh, R. R. Flores, Y. Zhu, Z. C. Schmiechen, R. W. Brooks, C. E. Trussoni, Y. Cui, L. Angelini, K.-A. Lee, S. J. McGowan, A. L. Burrack, D. Wang, Q. Dong, A. Lu, T. Sano, R. D. O'Kelly, C. A. McGuckian, J. I. Kato, M. P. Bank, E. A. Wade, S. P. S. Pillai, J. Klug, W. C. Ladiges, C. E. Burd, S. E. Lewis, N. F. La Russo, N. V. Vo, Y. Wang, E. E. Kelley, J. Huard, I. M. Stromnes, P. D. Robbins, L. J. Niedernhofer, An aged immune system drives senescence and ageing of solid organs. *Nature* **594**, 100–105 (2021).
35. N. Sayed, Y. Huang, K. Nguyen, Z. Krejciova-Rajaniemi, A. P. Grawe, T. Gao, R. Tibshirani, T. Hastie, A. Alpert, L. Cui, T. Kuznetsova, Y. Rosenberg-Hasson, R. Ostan, D. Monti, B. Lehallier, S. S. Shen-Orr, H. T. Maecker, C. L. Dekker, T. Wyss-Coray, C. Franceschi, V. Jojic, F. Haddad, J. G. Montoya, J. C. Wu, M. M. Davis, D. Furman, An inflammatory aging clock (iAge) based on deep learning tracks multimorbidity, immunosenescence, frailty and cardiovascular aging. *Nat. Aging* **1**, 598–615 (2021).
36. D. Saul, R. L. Kosinsky, E. J. Atkinson, M. L. Doolittle, X. Zhang, N. K. Le Brasseur, R. J. Pignolo, P. D. Robbins, L. J. Niedernhofer, Y. Ikeno, D. Jurk, J. F. Passos, L. T. J. Hickson, A. Xue, D. G. Monroe, T. Tchkonia, J. L. Kirkland, J. N. Farr, S. Khosla, A new gene set identifies senescent cells and predicts senescence-associated pathways across tissues. *Nat. Commun.* **13**, 4827 (2022).
37. J. C. Whitehead, B. A. Hildebrand, M. Sun, M. R. Rockwood, R. A. Rose, K. Rockwood, S. E. Howlett, A clinical frailty index in aging mice: Comparisons with frailty index data in humans. *J. Gerontol. A Biol. Sci. Med. Sci.* **69**, 621–632 (2014).
38. C. D. Camell, P. Günther, A. Lee, E. L. Goldberg, O. Spadaro, Y. H. Youm, A. Bartke, G. B. Hubbard, Y. Ikeno, N. H. Ruddle, J. Schultze, V. D. Dixit, Aging induces an Nlrp3 inflammasome-dependent expansion of adipose B cells that impairs metabolic homeostasis. *Cell Metab.* **30**, 1024–1039.e6 (2019).
39. V. Taneja, C. J. Krco, M. D. Behrens, H. S. Luthra, M. M. Griffiths, C. S. David, B cells are important as antigen presenting cells for induction of MHC-restricted arthritis in transgenic mice. *Mol. Immunol.* **44**, 2988–2996 (2007).
40. C. Tay, P. Kanellakis, H. Hosseini, A. Cao, B.-H. Toh, A. Bobik, T. Kyaw, B cell and CD4 T cell interactions promote development of atherosclerosis. *Front. Immunol.* **10**, 3046 (2019).
41. O. Altintas, S. Park, S. J. Lee, The role of insulin/IGF-1 signaling in the longevity of model invertebrates, *C. elegans* and *D. melanogaster*. *BMB Rep.* **49**, 81–92 (2016).
42. P. Makhijani, P. J. Basso, Y. T. Chan, N. Chen, J. Baechle, S. Khan, D. Furman, S. Tsai, D. A. Winer, Regulation of the immune system by the insulin receptor in health and disease. *Front. Endocrinol. (Lausanne)* **14**, 1128622 (2023).
43. D. A. Mogilenko, O. Shpynov, P. S. Andhey, L. Arthur, A. Swain, E. Esaulova, S. Brioschi, I. Shchukina, M. Kerndl, M. Bambouskova, Z. Yao, A. Laha, K. Zaitsev, S. Burdess, S. Gillfilan, S. A. Stewart, M. Colonna, M. N. Artyomov, Comprehensive profiling of an aging immune system reveals clonal $GZMK^+$ $CD8^+$ T cells as conserved hallmark of inflammaging. *Immunity* **54**, 99–115.e12 (2021).
44. J. D. Powell, K. N. Pollizzi, E. B. Heikamp, M. R. Horton, Regulation of immune responses by mTOR. *Annu. Rev. Immunol.* **30**, 39–68 (2012).
45. G. Desdin-Mico, G. Soto-Heredero, J. F. Aranda, J. Oller, E. Carrasco, E. Gabandé-Rodríguez, E. M. Blanco, A. Alfranca, L. Cussó, M. Desco, B. Ibañez, A. R. Gortazar, P. Fernández-Marcos, M. N. Navarro, B. Hernaez, A. Alcamí, F. Baixauli, M. Mittelbrunn, T cells with dysfunctional mitochondria induce multimorbidity and premature senescence. *Science* **368**, 1371–1376 (2020).
46. R. Selb, J. Eckl-Dorna, A. Neunkirchner, K. Schmetterer, K. Marth, J. Gamper, B. Jahn-Schmid, W. F. Pickl, R. Valenta, V. Niederberger, CD23 surface density on B cells is associated with IgE levels and determines IgE-facilitated allergen uptake, as well as activation of allergen-specific T cells. *J. Allergy Clin. Immunol.* **139**, 290–299.e4 (2017).
47. A. Getahun, F. Hjelm, B. Heyman, IgE enhances antibody and T cell responses in vivo via $CD23^+$ B cells. *J. Immunol.* **175**, 1473–1482 (2005).
48. N. Ron-Harel, G. Notarangelo, J. M. Ghergurovich, J. A. Paulo, P. T. Sage, D. Santos, F. K. Satterstrom, S. P. Gygi, J. D. Rabinowitz, A. H. Sharpe, M. C. Haigis, Defective respiration and one-carbon metabolism contribute to impaired naïve T cell activation in aged mice. *Proc. Natl. Acad. Sci. U.S.A.* **115**, 13347–13352 (2018).
49. M. Bodogai, J. O'Connell, K. Kim, Y. Kim, K. Moritoh, C. Chen, F. Gusev, K. Vaughan, N. Shulzhenko, J. A. Mattison, C. Lee-Chang, W. Chen, O. Carlson, K. G. Becker, M. Gurung, A. Morgun, J. White, T. Meade, K. Perdue, M. Mack, L. Ferrucci, G. Trinchieri, R. de Cabo, E. Rogaev, J. Egan, J. Wu, A. Biragyn, Commensal bacteria contribute to insulin resistance in aging by activating innate B1a cells. *Sci. Transl. Med.* **10**, eaat4271 (2018).
50. L. Yu, Q. Wan, Q. Liu, Y. Fan, Q. Zhou, A. A. Skowronski, S. Wang, Z. Shao, C. Y. Liao, L. Ding, B. K. Kennedy, S. Zha, J. Que, C. A. LeDuc, L. Sun, L. Wang, L. Qiang, IgG is an aging factor that drives adipose tissue fibrosis and metabolic decline. *Cell Metab.* **36**, 793–807.e5 (2024).
51. T. R. Valentino, N. Chen, P. Makhijani, S. Khan, S. Winer, X. S. Revelo, D. A. Winer, The role of autoantibodies in bridging obesity, aging, and immunosenescence. *Immun. Ageing* **21**, 85 (2024).
52. P. D. Pioli, D. Casero, E. Montecino-Rodriguez, S. L. Morrison, K. Dorshkind, Plasma cells are obligate effectors of enhanced myelopoiesis in aging bone marrow. *Immunity* **51**, 351–366.e6 (2019).
53. H. D. Chang, A. Radbruch, Maintenance of quiescent immune memory in the bone marrow. *Eur. J. Immunol.* **51**, 1592–1601 (2021).
54. N. Collins, S. J. Han, M. Enamorado, V. M. Link, B. Huang, E. A. Moseman, R. J. Kishton, J. P. Shannon, D. Dixit, S. R. Schwab, H. D. Hickman, N. P. Restifo, D. B. McGavern, P. L. Schwartzberg, Y. Belkaid, The bone marrow protects and optimizes immunological memory during dietary restriction. *Cell* **178**, 1088–1101.e15 (2019).
55. S. Tsai, X. Clemente-Casares, A. C. Zhou, H. Lei, J. J. Ahn, Y. T. Chan, O. Choi, H. Luck, M. Woo, S. E. Dunn, E. G. Engleman, T. H. Watts, S. Winer, D. A. Winer, Insulin receptor-mediated stimulation boosts T cell immunity during inflammation and infection. *Cell Metab.* **28**, 922–934.e4 (2018).
56. A. Mendoza, W. T. Yewdell, B. Hoyos, M. Schizas, R. Bou-Puerto, A. J. Michaels, C. C. Brown, J. Chaudhuri, A. Y. Rudensky, Assembly of a spatial circuit of T-bet-expressing T and B lymphocytes is required for antiviral humoral immunity. *Sci. Immunol.* **6**, eabi4710 (2021).
57. D. Wu, C. K. Wong, J. M. Han, P. C. Orban, Q. Huang, J. Gillies, M. Mojibian, W. T. Gibson, M. K. Levings, T reg-specific insulin receptor deletion prevents diet-induced and age-associated metabolic syndrome. *J. Exp. Med.* **217**, e20191542 (2020).
58. S. Ma, Z. Ji, B. Zhang, L. Geng, Y. Cai, C. Nie, J. Li, Y. Zuo, Y. Sun, G. Xu, B. Liu, J. Ai, F. Liu, L. Zhao, J. Zhang, H. Zhang, S. Sun, H. Huang, Y. Zhang, Y. Ye, Y. Fan, F. Zheng, J. Hu, B. Zhang, J. Li, X. Feng, F. Zhang, Y. Zhuang, T. Li, Y. Yu, Z. Bao, S. Pan, C. Rodriguez Esteban, Z. Liu, H. Deng, F. Wen, M. Song, S. Wang, G. Zhu, J. Yang, T. Jiang, W. Song, J. C. Izpisua Belmonte, J. Qu, W. Zhang, Y. Gu, G. H. Liu, Spatial transcriptomic landscape unveils immunoglobin-associated senescence as a hallmark of aging. *Cell* **187**, 7025–7044.e34 (2024).
59. F. Barrow, S. Khan, G. Fredrickson, H. Wang, K. Dietsche, P. Parthiban, S. Robert, T. Kaiser, S. Winer, A. Herman, O. Adeyi, M. Mouzaki, A. Khoruts, K. A. Hogquist, C. Staley, D. A. Winer, X. S. Revelo, Microbiota-driven activation of intrahepatic B cells aggravates NASH through innate and adaptive signaling. *Hepatology* **74**, 704–722 (2021).
60. J. Rip, M. J. W. de Bruijn, A. Kaptein, R. W. Hendriks, O. B. J. Corneth, Phosphoflow protocol for signaling studies in human and murine B cell subpopulations. *J. Immunol.* **204**, 2852–2863 (2020).
61. H. Luck, S. Khan, J. H. Kim, J. K. Copeland, X. S. Revelo, S. Tsai, M. Chakraborty, K. Cheng, Y. T. Chan, M. K. Nøhr, X. Clemente-Casares, M.-C. Perry, M. Ghazarian, H. Lei, Y.-H. Lin, B. Coburn, A. Okrainec, T. Jackson, S. Poutanen, H. Gaisano, J. P. Allard, D. S. Guttman, M. E. Conner, S. Winer, D. A. Winer, Gut-associated IgA^+ immune cells regulate obesity-related insulin resistance. *Nat. Commun.* **10**, 3650 (2019).
62. Y. Hao, S. Hao, E. Andersen-Nissen, W. M. Mauck III, S. Zheng, A. Butler, M. J. Lee, A. J. Wilk, C. Darby, M. Zager, P. Hoffman, M. Stoeckius, E. Papalexi, E. P. Mimitou, J. Jain, A. Srivastava, T. Stuart, L. M. Fleming, B. Yeung, A. J. Rogers, J. M. McElrath, C. A. Blish, R. Gottardo, P. Smibert, R. Satija, Integrated analysis of multimodal single-cell data. *Cell* **184**, 3573–3587.e29 (2021).
63. I. Tirosh, B. Izar, S. M. Prakadan, Wadsworth MH 2nd, D. Treacy, J. J. Trombetta, A. Rotem, C. Rodman, C. Lian, G. Murphy, M. Fallahi-Sichani, K. Dutton-Regester, J. R. Lin, O. Cohen, P. Shah, D. Lu, A. S. Genshaft, T. K. Hughes, C. G. Ziegler, S. W. Kazer, A. Gaillard, K. E. Kolb, A. C. Villani, C. M. Johannessen, A. Y. Andreev, E. van Allen, M. Bertagnolli, P. K. Sorger, R. J. Sullivan, K. T. Flaherty, D. T. Frederick, J. Jané-Valbuena, C. H. Yoon,

O. Rozenblatt-Rosen, A. K. Shalek, A. Regev, L. A. Garraway, Dissecting the multicellular ecosystem of metastatic melanoma by single-cell RNA-seq. *Science* **352**, 189–196 (2016).
64. R. Satija, J. A. Farrell, D. Gennert, A. F. Schier, A. Regev, Spatial reconstruction of single-cell gene expression data. *Nat. Biotechnol.* **33**, 495–502 (2015).
65. C. S. McGinnis, L. M. Murrow, Z. J. Gartner, DoubletFinder: Doublet detection in single-cell RNA sequencing data using artificial nearest neighbors. *Cell Syst.* **8**, 329–337.e4 (2019).
66. S. He, L.-H. Wang, Y. Liu, Y.-Q. Li, H.-T. Chen, J.-H. Xu, W. Peng, G.-W. Lin, P.-P. Wei, B. Li, X. Xia, D. Wang, J.-X. Bei, X. He, Z. Guo, Single-cell transcriptome profiling of an adult human cell atlas of 15 major organs. *Genome Biol.* **21**, 294 (2020).
67. S. C. van den Brink, A. Alemany, V. van Batenburg, N. Moris, M. Blotenburg, J. Vivié, P. Baillie-Johnson, J. Nichols, K. F. Sonnen, A. M. Arias, A. van Oudenaarden, Single-cell and spatial transcriptomics reveal somitogenesis in gastruloids. *Nature* **582**, 405–409 (2020).
68. Z. A. Clarke, G. D. Bader, MALAT1 expression indicates cell quality in single-cell RNA sequencing data. bioRxiv 2024.07.14.603469 [Preprint] (2024). https://doi.org/10.1101/2024.07.14.603469.
69. G. Finak, A. McDavid, M. Yajima, J. Deng, V. Gersuk, A. K. Shalek, C. K. Slichter, H. W. Miller, M. J. McElrath, M. Prlic, P. S. Linsley, R. Gottardo, MAST: A flexible statistical framework for assessing transcriptional changes and characterizing heterogeneity in single-cell RNA sequencing data. *Genome Biol.* **16**, 278 (2015).
70. A. Subramanian, P. Tamayo, V. K. Mootha, S. Mukherjee, B. L. Ebert, M. A. Gillette, A. Paulovich, S. L. Pomeroy, T. R. Golub, E. S. Lander, J. P. Mesirov, Gene set enrichment analysis: A knowledge-based approach for interpreting genome-wide expression profiles. *Proc. Natl. Acad. Sci. U.S.A.* **102**, 15545–15550 (2005).
71. C. Trapnell, D. Cacchiarelli, J. Grimsby, P. Pokharel, S. Li, M. Morse, N. J. Lennon, K. J. Livak, T. S. Mikkelsen, J. L. Rinn, The dynamics and regulators of cell fate decisions are revealed by pseudotemporal ordering of single cells. *Nat. Biotechnol.* **32**, 381–386 (2014).
72. X. Qiu, A. Hill, J. Packer, D. Lin, Y.-A. Ma, C. Trapnell, Single-cell mRNA quantification and differential analysis with Census. *Nat. Methods* **14**, 309–315 (2017).
73. K. L. Howe, P. Achuthan, J. Allen, J. Allen, J. Alvarez-Jarreta, M. R. Amode, I. M. Armean, A. G. Azov, R. Bennett, J. Bhai, K. Billis, S. Boddu, M. Charkhchi, C. Cummins, L. da Rin Fioretto, C. Davidson, K. Dodiya, B. el Houdaigui, R. Fatima, A. Gall, C. Garcia Giron, T. Grego, C. Guijarro-Clarke, L. Haggerty, A. Hemrom, T. Hourlier, O. G. Izuogu, T. Juettemann, V. Kaikala, M. Kay, I. Lavidas, T. le, D. Lemos, J. Gonzalez Martinez, J. C. Marugán, T. Maurel, A. McMahon, S. Mohanan, B. Moore, M. Muffato, D. N. Oheh, D. Paraschas, A. Parker, A. Parton, I. Prosovetskaia, M. P. Sakthivel, A. I. A. Salam, B. M. Schmitt, H. Schuilenburg, D. Sheppard, E. Steed, M. Szpak, M. Szuba, K. Taylor, A. Thormann, G. Threadgold, B. Walts, A. Winterbottom, M. Chakiachvili, A. Chaubal, N. de Silva, B. Flint, A. Frankish, S. E. Hunt, G. R. IIsley, N. Langridge, J. E. Loveland, F. J. Martin, J. M. Mudge, J. Morales, E. Perry, M. Ruffier, J. Tate, D. Thybert, S. J. Trevanion, F. Cunningham, A. D. Yates, D. R. Zerbino, P. Flicek, Ensembl 2021. *Nucleic Acids Res.* **49**, D884–D891 (2021).
74. S. Rahmati, M. Abovsky, C. Pastrello, M. Kotlyar, R. Lu, C. A. Cumbaa, P. Rahman, V. Chandran, I. Jurisica, pathDIP 4: An extended pathway annotations and enrichment analysis resource for human, model organisms and domesticated species. *Nucleic Acids Res.* **48**, D479–D488 (2020).

Acknowledgments: We thank Princess Margaret Genomics Centre (PMGC) for help in single-cell sequencing and the Princess Margaret Hospital (PMH) flow core for assistance with flow cytometry and cell sorting. We thank H. Lei for help early on in mouse colony breeding and maintenance. Graphical illustrations were made via BioRender.com. **Funding:** This work was supported in part through funds derived from the NIH grant R01DK128435 (D.A.W.); the Canadian Institutes of Health Research (CIHR) grants FDN-148385, PJT-186165, PJT-195795, and PJT-169175 (D.A.W.); and Mount Sinai Hospital (S.W.). I.J. was supported in part by funding from Natural Sciences Research Council (NSERC no. 203475), Canada Foundation for Innovation (CFI nos. 225404 and 30865), Ontario Research Fund (RDI no. 34876), IBM, and Ian Lawson van Toch Fund. This project was also supported by funds derived from an Impetus Longevity Grant from Norn Group, awarded to S.K. S.K. is also a recipient of the Queen Elizabeth II Graduate Scholarship in Science and Technology (QEII- GSST)/Aventis Pasteur and the Dick and Peggy Sharpe Student Fellowship in Immunology. **Author contributions:** Conceptualization: S.K., M.C., S.W., and D.A.W. Investigation: S.K., M.C., N.C., T.W., Y.T.C., and F.J.A. Computational analysis: F.W., A.S., and M.K. Supervision: M.W., R.-K.L., M.H., I.J., A.J.G., P.S.O., D.F., S.T., S.W., and D.A.W. Writing: S.K., M.C., S.W., and D.A.W. **Competing interests:** The authors declare that they have no competing interests. **Data, code, and materials availability:** Raw data for RNA sequencing analyses and associated codes have been deposited in the National Centre for Biotechnology Information Genome Expression Omnibus (GSE275967). Primer sequences and antibody supplier and catalog numbers are provided in tables S1 and S2. Tabulated data underlying the figures are provided in data file S1. All other data needed to evaluate the conclusions in the paper are present in the paper or the Supplementary Materials. All materials are commercially available.

Submitted 6 January 2025
Resubmitted 4 July 2025
Accepted 8 January 2026
Published 30 January 2026
10.1126/sciimmunol.adv7615

Science Immunology

B cells drive CD4 T cell immunosenescence and age-associated health decline

Saad Khan, Mainak Chakraborty, Fei Wu, Nan Chen, Tao Wang, Yi Tao Chan, Azin Sayad, Max Kotlyar, Faisal J. Alibhai, Minna Woo, Ren-Ke Li, Mansoor Husain, Igor Jurisica, Adam J. Gehring, Pamela S. Ohashi, David Furman, Sue Tsai, Shawn Winer, and Daniel A. Winer

Sci. Immunol. **11** (115), eadv7615. DOI: 10.1126/sciimmunol.adv7615

Editor's summary

Immunosenescence is the gradual age-associated decline in immune system function that renders older adults more susceptible to infection and disease. However, the mechanisms driving immunosenescence remain poorly understood. Khan *et al.* found that B cell–deficient mice maintain a CD4 T cell compartment that resists age-related decline and exhibit improved overall health, including an extended life span, compared with control mice. Aged B cell–deficient mice displayed fewer signs of CD4 T cell immunosenescence, including more naïve T cells, enhanced activation capacity, and reduced clonal restriction. These effects were mediated in part by B cell insulin receptor signaling and MHCII, identifying a pathway through which aging B cells can promote CD4 T cell immunosenescence. –Claire Olingy